Brady Esther C. (Orcid ID: 0000-0001-7833-2249)
Stevenson Samantha (Orcid ID: 0000-0002-1223-8521)
Bailey David Anthony (Orcid ID: 0000-0002-6584-0663)
Noone David (Orcid ID: 0000-0002-8642-7843)
Nusbaumer Jesse (Orcid ID: 0000-0002-4370-3537)
Otto-Bliesner Bette L (Orcid ID: 0000-0003-1911-1598)
Tabor Clay R (Orcid ID: 0000-0002-9915-6157)
Wong Tony E (Orcid ID: 0000-0002-7304-3883)
Zhang Jiaxu (Orcid ID: 0000-0002-8564-3026)
Zhu Jiang (Orcid ID: 0000-0002-0908-5130)

The connected isotopic water cycle in the Community Earth System Model version 1

Brady, E.[1], Stevenson, S*.[2], Bailey, D.[1], Liu, Z.[3], Noone, D.[4], Nusbaumer, J.[5], Otto-Bliesner, B.L.[1], Tabor, C.[6], Tomas, R.[1], Wong, T.[7], Zhang, J.[8], Zhu, J.[9]

[1]Climate & Global Dynamics Laboratory, National Center for Atmospheric Research, Boulder, CO USA

[2]Bren Hall 2400, Bren School of Environmental Science & Management, University of California, Santa Barbara, Santa Barbara, CA USA 93107

[3]Department of Geography, The Ohio State University, Columbus, OH USA

[4]College of Earth, Ocean, & Atmospheric Sciences, Oregon State University, Corvallis, OR USA

[5]NASA Goddard Institute for Space Studies and Center for Climate Systems Research, Columbia University, New York, NY USA

[6]Department of Geosciences, University of Connecticut, Storrs, CT USA

[7]Department of Computer Science, University of Colorado at Boulder, Boulder, CO USA

[8]Center for Nonlinear Studies, Los Alamos National Laboratory, Los Alamos, NM USA

[9]Department of Earth and Environmental Sciences, University of Michigan, Ann Arbor, MI USA

Key Points

- **An isotope-enabled version of the Community Earth System Model (iCESM1) is now publicly available.**

This is the author manuscript accepted for publication and has undergone full peer review but has not been through the copyediting, typesetting, pagination and proofreading process, which may lead to differences between this version and the Version of Record. Please cite this article as doi: 10.1029/2019MS001663

- **iCESM1 simulates the major observed features of d18O and dD over the late 20th century.**
- **iCESM1 is useful for both modern climate and paleoclimate applications.**

Abstract

Because of the pervasive role of water in the Earth system, the relative abundances of stable isotopologues of water are valuable for understanding atmospheric, oceanic and biospheric processes, and for interpreting paleoclimate proxy reconstructions. Isotopologues are transported by both large-scale and turbulent flows, and the ratio of heavy to light isotopologues changes due to fractionation that can accompany condensation and evaporation processes. Correctly predicting the isotopic distributions requires resolving the relationships between large-scale ocean and atmospheric circulation and smaller-scale hydrological processes, which can be accomplished within a coupled climate modeling framework. Here we present the water isotope-enabled version of the Community Earth System Model version 1 (iCESM1), which simulates global variations in water isotopic ratios in the atmosphere, land, ocean, and sea ice. In a transient Last Millennium simulation covering the 850–2005 period, iCESM1 correctly captures the late 20th century structure of $\delta^{18}O$ and δD over the global oceans, with more limited accuracy over land. The relationship between salinity and seawater $\delta^{18}O$ is also well represented over the observational period, including inter-basin variations. We illustrate the utility of coupled, isotope-enabled simulations using both Last Millennium simulations and freshwater hosing experiments with iCESM1. Closing the isotopic mass balance between all components of the coupled model provides new confidence in the underlying depiction of the water cycle in CESM, while also highlighting areas where the underlying hydrologic balance can be improved. The iCESM1 is poised to be a vital community resource for ongoing model development with both modern and paleoclimate applications.

1. Introduction

The isotopic ratios of hydrogen and oxygen in water (i.e., ^{16}O /^{18}O, H/D) are affected by processes throughout the hydrological cycle, including: isotopic fractionation during evaporation, condensation and isotopic exchange between raindrops and the surrounding vapor; interaction between large-scale and turbulent-scale transport; and variation in moisture source regions (Craig 1961; Craig and Gordon 1965; Dansgaard 1964; Epstein et al. 1965; Gat 2000; Galewsky et al, 2016). The relative abundances of stable isotopes (given by the isotope ratios, R, and hereafter denoted by delta notation, $\delta^{18}O$ and δD, where $\delta = (R/R_s - 1)\times 1000$ and R_s is the isotope ratio of the international standard reference material) are sensitive tracers of hydrological activity, which provide valuable tools for inferring atmospheric circulation (e.g., Noone, 2008; Aggarwal et al. 2016; Dee et al. 2018). Because of the large spatial and temporal scales of the relevant processes, isotope ratios often provide more robust information on large-scale circulation than more commonly observed physical variables such as precipitation, which is often strongly affected by localized processes (Konecky et al. 2013; Hu et al. 2018). As such, the observational community is beginning to leverage these capacities of water isotopes (Kuang et al. 2003, Berkelhammer et al. 2012, Noone 2012, Tremoy et al. 2014, Galewsky et al. 2016).

Understanding the controls on isotope ratios is critical in paleoclimate research. Most 'proxy' reconstructions are made using measurements of isotopic ratios in natural archives such as ice cores (e.g., Epstein and Mayeda 1965; Dansgaard et al. 1993; Petit et al. 1999; North Greenland Eemian Ice Drilling Project (NEEM) community members, 2013), corals (e.g., Cobb et al. 2003, 2013), speleothems (e.g., Wang et al. 2001), and marine and lake sediments (e.g., Zachos et al. 2001). Most of these archives are intricately reliant on isotope ratios in the water cycle. As such, using proxy records to interpret past climate variations in the atmosphere and ocean requires not only an understanding of the proxy system (reef, speleothem, etc.; Evans et al. 2013), but also of how physical variables (temperature, precipitation, soil moisture, etc.) lead to changes in the isotopic expression at the location of the proxy site. This has been estimated using empirical relationships in observations (e.g., Moerman et al. 2014; Dee et al. 2018), but a detailed physical understanding requires the use of climate models with the capacity to directly simulate water isotope ratios.

Efforts to simulate water isotope ratios in climate models span at least half a decade. Earlier isotope-enabled simulations typically included only the atmosphere and land surface (Joussaume et al, 1984; Jouzel et al. 1987; Jouzel et al. 1991; Hoffmann et al. 1998; Mathieu et al. 2002; Noone and Simmonds, 2002; Werner et al. 2011; Noone and Sturm 2010; Field et al. 2014), and have been found to be reliable in reproducing the extensive database of precipitation observations from the Global Network for Isotopes in Precipitation (GNIP). There are fewer more recent atmospheric models with isotopic tracers that have been compared to isotope ratios of tropospheric water vapor from satellite or in situ observations (notably, Schmidt et al. 2005, Risi et al. 2012; Nusbaumer et al. 2017). Water isotope ratios have also been included in ocean

general circulation models (OGCMs; Schmidt, 1998, 1999; Paul et al. 1999; Delaygue et al. 2000) and used for constructing past and present three-dimensional tracer fields (Wadley et al. 2002). Some efforts to understand the diversity of simulated isotopic variations across models have also been completed, most prominently through the Stable Water Isotope Intercomparison Group (SWING2) project (Risi et al. 2012; Conroy et al. 2013).

With the recognition of the importance of coupled dynamics, there is also focus on coupled isotope-enabled simulations. Intermediate-complexity coupled models such as SPEEDY-IER (Dee et al. 2015) and iLOVECLIM (Roche et al. 2013; Caley & Roche 2013) are computationally inexpensive, but do not include many important processes such as atmospheric convection/cloud formation, land surface processes, and sea ice effects. As such, the use of fully-coupled GCMs has gained popularity (Schmidt et al. 2007; LeGrande & Schmidt 2008; Tindall et al. 2009; Risi et al. 2010; Russon et al. 2013; Werner et al. 2016). However, increasing the number of isotope-enabled GCMs is critical, as the diversity of model representations of both mean climate and climate variability is well documented for both physical and isotopic variables (Risi et al. 2012; Conroy et al. 2013; Stevenson, 2012). Additionally, no systematic intercomparisons of newer isotope-enabled model versions have been completed since SWING2. Thus, the degree to which recent model improvements lead to enhanced capacity for correctly capturing isotopic variability remains an open question. These model improvements are substantial in many cases; for instance, the simulation of the El Nino/Southern Oscillation (ENSO) has improved drastically in the Community Earth System Model (CESM1; Bellenger et al. 2014) relative to previous model versions (e.g. the Community Climate System Model version 4; Gent et al. 2011), and it is expected that these types of advances will lead to corresponding improvements in the isotopic simulation.

Here we present a new version of CESM1 (Hurrell et al. 2013), including the capacity to simulate hydrogen and oxygen isotope ratios in the water cycle and both abiotic radiocarbon and biotic $^{13}C/^{14}C$ ocean tracers (Jahn et al. 2015). The CESM is one of the most widely-used climate models in the world, owing to its unique open-source nature and the availability of publicly hosted community ensemble simulations (Kay et al. 2016; Otto-Bliesner et al. 2016). However, although some components of the previous model versions (e.g. CCM3, CAM2, CAM3) have included isotopic simulation capacity (e.g., Tharammal et al. 2013; Guan et al. 2016), to date no isotopic processes had been included in the fully coupled CESM. This new model version (hereafter 'iCESM1') thus represents a significant technical advance, as the isotopic simulation capabilities will be retained through successive model generations. iCESM1 is already being used in a variety of contexts, including the water isotope-enabled simulation of the Last Glacial Maximum (Zhu et al. 2017a), freshwater hosing experiments to mimic the Heinrich-like events (Zhu et al. 2017b), orbital-driven monsoon variability (Tabor et al. 2018), and the creation of an isotope-enabled Last Millennium community ensemble analogous to the CESM Last Millennium Ensemble (Otto-Bliesner et al. 2016).

2. Model Description

A diagram of the iCESM1 model components and moisture fluxes is shown in Figure 1. The isotope-enabled model has as its base the CESM1.2 release (http://www.cesm.ucar.edu/models/cesm1.2/), which has active atmosphere, land, ocean, river transport, and sea ice component models linked through a coupler. The atmosphere component model is the Community Atmosphere Model, version 5.3 (CAM5.3; Neale et al. 2010) and the land component is the Community Land Model, version 4 (CLM4; Oleson et al. 2010). Here, we adopt the "FV2" version of CESM, where "FV2" refers to the finite-volume dynamical core and the nominal 2º resolution. (The FV2 CESM has a horizontal resolution of 1.9º in latitude and 2.5º in longitude.) The ocean and sea ice components are the Parallel Ocean Program version 2 (POP2; Smith et al. 2010) and the Los Alamos Sea Ice Model version 4 (CICE4; Hunke et al. 2010). POP2 and CICE4 here use a common grid of size 320×384, a displaced-pole grid with poles in Greenland and Antarctica, and a nominal 1º resolution with enhancement near the equator and in the North Atlantic. A River Transport Model (RTM) routes total runoff from the land surface model to either the active ocean or marginal seas, enabling the hydrological cycle to be closed. This version of CESM has been previously shown to well simulate preindustrial and present-day climate (e.g., Hurrell et al. 2013; Kay et al. 2015; Otto-Bliesner et al. 2016).

Water isotope ratios, and the associated fluxes and isotopic fractionations, are tracked in all of the components of the hydrologic cycle: atmospheric water vapor and clouds, soil moisture and other land surface water pools, oceans, and sea ice. Fractionation describes the vapor pressure dependent equilibrium fractionation, or the mass dependent kinetic fractionation that accompanies molecular diffusion. Due to fractionation effects, isotopic species respond slightly differently to hydrologic processes (e.g. through different rates of evaporation and associated latent heating/cooling). However, the resulting differences in isotope ratios are assumed to have negligible influence on latent heating or heat capacity and are not large enough to directly impact the hydrologic cycle itself, nor its interactions with the rest of the climate system. Thus, the first step in representing water isotopes in a climate model is to create a new, parallel hydrologic cycle for the isotope tracers. This diagnostic hydrologic cycle experiences all the same changes and processes that the regular water cycle does, but has no influence on any other underlying simulation of the predicted state of the model. The simulated water isotopes are represented as numerical "water tracers"; they track water through space and time, through the different phases of water, and the different components of the hydrologic cycle (e.g., Bosilovich 2004, Noone and Simmonds 2002b; Risi et al. 2010; Singh et al. 2017a,b; Dyer et al. 2018). This secondary water tracer cycle has been implemented in all components of CESM, except land ice, along with the necessary fractionation physics routines.

iCESM is designed to ensure that the physics governing isotopic and other physical variables correspond as closely as possible with one another. This means requiring that certain isotope-specific processes respond directly to simulated physical processes, rather than tuning to match isotopic observations. For example, isotopic fractionation during rain re-evaporation is sometimes tuned to minimize the simulated isotopic error by prescribing a certain evaporation

fraction (e.g. Jouzel et al. 1987, 1992; Hoffmann et al. 1998). By contrast, in iCESM this fractionation is governed directly by the precipitation flux simulated by the model. Following model physics rather than separately tuning isotopic processes may result in larger disagreement with observations in some cases; however, it allows water isotope observations to be more easily used to evaluate the underlying model physics. This is particularly valuable given the recent advent of global datasets from satellite instruments and high-frequency in-situ spectrometer measurements (for a recent survey of isotope ratio datasets, see Galewsky et al. 2016). These datasets provide the potential to constrain global physical processes using water isotope ratios (Schmidt et al. 2005; Bony et al. 2008; Field et al. 2014), and to improve future versions of CESM (Nusbaumer et al. 2017).

Water tracers can also be used as water "tags" in the atmosphere and ocean, where aspects of the secondary water tracer hydrologic cycle are turned off for a particular tracer to isolate, or "tag", a specific region or process. Water tags have a long history of use in climate and weather models, as they allow for the detailed evaluation of moisture sources and sinks (Koster et al. 1986; Noone and Simmonds, 2002; Sodemann et al. 2009; Lewis et al. 2010; Dominguez et al. 2016; Zhang et al. 2017). Water tagging has been implemented in the atmospheric component of CESM with new infrastructure within CAM and CLM to facilitate a variety of applications. For instance, the scheme has already been used to examine global (Singh et al. 2016) and regional (Dyer et al. 2017) variations in moisture source, as well as to determine the average moisture sources for specific weather phenomena (Nusbaumer and Noone, 2018). This water tagging can be applied to water isotopologues as well, allowing one to determine the impact of moisture source and pathway changes on the isotope ratios for a particular region (Tabor et al. 2018; Zhu et al. 2017b). We note that water tagging currently requires custom coding within the coupler to enable tag information to pass between components, and in the default configuration iCESM has tags within each of CAM5, CLM4, and POP2 as independent components (i.e., tags are not coupled).

2.1. Atmosphere model

The atmospheric component of iCESM1 is the isotope-enabled Community Atmosphere Model version 5.3 (iCAM5.3), which is based on the original, non-isotope enabled CAM5 (Neale et al. 2010). iCAM5.3 includes an additional, passive tracer hydrologic cycle that follows standard "bulk" model water in all phases through surface fluxes and boundary layer mixing, shallow convection, deep convection, cloud macro- and micro-physics, and advection via the resolved large-scale atmospheric dynamics. The isotopic water vapor model state variable is proportional to specific humidity, and described as $q_i = \gamma R/R_s\, q$, where q is the specific humidity, subscript i denotes the isotopologue, γ is the number of possible isotopic substitution sites in water (1 for ^{18}O and 2 for ^{2}H), R is the molar ratio between the heavy and light isotopologue or water tracer, and R_s is a isotope ratio of an appropriate standard. It is useful to choose R_s to be the

international standard (i.e., V-SMOW), which ensures similar numerical truncation error for the bulk water and isotopic species while also preserving mass during advection. This hydrologic cycle can be used to simulate both water tracers or tags and water isotopes, and therefore can track the isotope ratio of tagged water. The isotopic scheme is built on the same philosophy as previous isotopic models (especially, Jouzel et al. 1987; Hoffmann et al. 1998; Noone and Simmonds 2002a; Noone and Sturm 2008), and modified to match the more sophisticated cloud schemes in CAM5 relative to prior models.

For water isotopologues, equilibrium fractionation occurs whenever there is a phase change of water, except for the sublimation of ice directly into vapor. In both convective and stratiform clouds, cloud liquid is assumed to be maintained in equilibrium with interstitial vapor. Ice is deposited from vapor (onto small crystals or snow) and is accompanied by a kinetic effect (Jouzel and Merlivat, 1984). No fractionation occurs during melting or freezing of ice and liquid condensate (cloud and falling precipitation). The Wegner-Bergeron-Findisen process is treated as a special case to model the isotopic effects for transition from liquid to ice via vapor phase in mixed phase clouds. This is accompanied by kinetic fractionation during re-deposition of the newly evaporated vapor onto ice. Isotopic exchange occurs as rain drops fall and follows the approach outlined by Stewart (1975) that describes the approach toward equilibrium that is mediated by the diffusive flux adjusted for ventilation effects. This expression of diffusion provides a kinetic fractionation as drops fall. The amount of isotopic equilibration between rain drops and vapor that occurs is a function of rain drop size, which is itself estimated from the rain rate. Thus, high rain rates result in large drop sizes and partial equilibration, while low rain rates result in small drop sizes and (near-)complete equilibration. Both equilibrium and kinetic fractionation occurs during surface ocean evaporation based on a Craig and Gordon (1965) approach modified to include kinetic effects (Merlivat and Jouzel, 1979). A change was made to the CAM5.3 formulation to track both ice and liquid within convective updrafts (rather than just total condensate), which facilitates a different ice formation pathways and detrainment of both ice and liquid to the environment. This change was required to allocate detrained condensate to ice and liquid stratiform cloud. A more in-depth description of the isotopic physics, along with an analysis of iCAM5.3 results compared to observations, can be found in Nusbaumer et al. (2017).

2.2 Land model

The Community Land Model, version 4 (CLM4; Oleson et al. 2010) is used as the land surface component of iCESM. CLM4 is a one-dimensional surface model of the energy, momentum, water, and CO_2 exchanges between land and atmosphere. CLM4 accounts for ecosystem dynamics, biophysical, hydrological, and biogeochemical processes based on plant functional types (PFTs). The isotope-enabled version of CLM4, iCLM4, contains a parallel water isotopic hydrology that is similar to the implementation in CAM5, and the isotopic fractionation scheme follows a similar philosophy as was used in an earlier NCAR Land Surface Model (LSM) (Riley et al. 2002; Noone et al, 2002; Buenning et al. 2011; Kanner et al. 2014). The native CLM4

stores water in four pools: soil liquid water and ice, snowpack, and moisture intercepted by the vegetation canopy.

As in CAM5, the state variable carried for isotope tracers is proportional to the product of the isotope ratio and the primary state variable, with accompanying isotopic fluxes. Liquid water transport in the soil results from solution of an approximate Richards equation, and the isotopic tracer transport follows the diagnosed fluxes without fractionation. Melt and freeze of below and above ground water occurs with no fractionation, and the transport of isotopic tracers within the snowpack follows that of bulk water with no fractionation. It was found for stability of the solution in locations near ice margins, frost must be formed without fractionation to avoid sequential enrichment over a series of diel cycles of frost and sublimation. Snow pack has a maximum depth of one meter (water equivalent) over continental ice and ice sheets. In both Greenland and Antarctica this represents several years of accumulation. Furthermore, if the incident snow and precipitation would lead a gridcell to exceed the one meter water equivalent maximum in the snowpack, the excess water is channeled into runoff with the isotopic ratio of the incident water (no mixing with the existing water in the snowpack). For isotopic fractionation during evaporation and sublimation from snowpack (more than 10 mm of accumulation), only the isotope ratio of the top snow layer is included. These choices are made to remain consistent with the native CLM4 model physics.

For vegetated PFTs iCLM4 uses an implicit solver to maintain a five-way water isotopic flux balance between the total land surface evapotranspiration flux and the sum of (1) surface evaporation, (2) evaporation of canopy-intercepted water, and transpiration from sunlit (3) and shaded (4) leaves, and (5) export of water vapor from the canopy airspace to the atmosphere above. An implicit scheme is used to maintain stability of the upper layer soil water and canopy intercepted water in cases where the evaporation is near complete. At each timestep, the updated water isotope ratios are calculated to satisfy this mass balance.

It is assumed that transpired water has the same isotope ratio as the root-weighted soil water, while the isotope ratio of leaf water is set by the requirement of isotopic mass balance within the plant (i.e., water mass in plants is constant, and small compared to transpiration flux). The non-vegetated case is a simplification of this five-way balance that excludes transpiration. Evaporation from soil includes kinetic fractionation based on both aerodynamic and soil diffusive transport. Transpiration includes kinetic fractionation due to aerodynamic transport from the canopy, though a leaf boundary layer and due to stomatal conductance. Evaporation from soil includes kinetic fractionation based on both aerodynamic and soil diffusive transport. No fractionation process takes place in the isotope-enabled River Transport Model (iRTM). The isotopic river runoff is simply routed to the ocean, as is done for the bulk water (Oleson et al. 2010). The interested reader is referred to Wong et al. (2017) for further details regarding iCLM4.

2.3 Ocean model

The ocean component of the iCESM1 is based on the isotope-enabled, stand-alone POP2 (iPOP2) (Zhang et al. 2017). Water isotopes are transported by both resolved flow and parameterized (diffusive) turbulence in the ocean interior as a passive tracer. The model simulated surface seawater isotope ratios are used to compute evaporation. Freshwater fluxes represented are evaporation, precipitation, river runoff, and sea ice formation, with an option to include an additional surface freshwater flux to account for glacial discharge in paleoclimate applications. These isotopic fluxes are passed through the coupler and used to construct a surface boundary condition for the isotopic water tracers. The global ocean volume is fixed in POP2, which requires the use of a "virtual isotopic flux", analogous to the virtual salt flux, in the implementation of the surface boundary condition. Bulk and isotopic water fluxes of evaporation, precipitation, runoff and freezing and melting of ice received by the ocean are converted into a virtual isotopic flux applied to the top ocean layer.

Following the marginal sea balancing scheme for the bulk surface freshwater flux and salinity in the standard POP (Smith et al. 2010), a parallel isotopic marginal sea balancing scheme has been implemented in iPOP2 for the isotopic surface water flux and seawater isotope ratios. Unlike the surface heat flux and SST, there is no direct negative feedbacks between the surface freshwater flux and salinity. As a result, POP2 could produce unphysical salinity in isolated marginal sea regions (e.g., a negative salinity in marginal seas with large freshwater input from river runoff). To mitigate this issue, the standard POP2 implements a marginal sea balancing scheme, which transports any excess/deficit of freshwater flux over a marginal sea to the nearby open ocean (Smith et al. 2010). This method implicitly connects marginal seas with the active ocean and conserves the total water in the system. We have implemented a parallel marginal sea balancing scheme for the isotopic water flux and seawater isotope ratios, in which any excess/deficit of isotopic water flux over a marginal sea is re-directed to the nearby open ocean, an effort to remove any unrealistic seawater isotope ratios over the marginal seas. As in standard POP2, marginal seas in a modern climate configuration of iPOP2 include the Red Sea, the Baltic Sea, the Black Sea and the Caspian Sea.

2.4 Sea ice model

Water isotope tracers in iCICE4 are treated similarly to other tracer concentrations. Just as in standard CICE4, the sinks of the isotopic water mass in the sea ice-snow system are top, bottom and lateral melting and sublimation. The sources include snowfall, congelation and frazil sea-ice growth, and vapor condensation. Snow is converted to sea ice when flooded with seawater. In addition to these thermodynamic changes, the sea ice dynamics transport the isotopes; these are conserved in the advection scheme. The subgridscale ice thickness distribution will redistribute the isotopes between thickness categories, but the overall gridcell concentration is not changed.

Currently, fractionation in iCICE4 is applied during vapor condensation and sea-ice formation. The condensation includes any "negative evaporation" over snow covered and bare sea ice. The fractionation coefficients for vapor condensation were adopted from Majoube (1971). The formation of sea ice (both congelation and frazil) in iCICE4 follows an equilibrium fractionation process (Lehmann and Siegenthaler, 1991). The uptake of a water isotopologue is a product of the mass of new bulk sea ice, isotopic ratio of the surface seawater and the corresponding fractionation coefficient. Sea-ice melting occurs without fractionation. Rainfall over sea ice, including the isotopic information, is not accumulated on the sea ice and is passed to the ocean directly by the model.

2.5 The coupling and optional flux correction

The CESM coupler passes information on isotopic water fluxes and state variables between components using the same methodology as for bulk water. Each model sends relevant fields and fluxes necessary for coupling the isotopic hydrologic cycle on their respective grids to the coupler. These isotopic water fluxes and state variables are re-mapped and merged for the exchange on the appropriate grid, and sent to each model for use in driving the isotopic hydrologic cycle. Details about the computation of isotopic evaporation over the sea surface can be found in Nusbaumer et al. (2017).

By design, iCESM1 conserves (to the order of the numerical schemes) the total water mass and total isotopologue mass within all components. This requires some care in setting model initial conditions that match natural abundances. In practice this has been accomplished in an ad hoc manner by allowing each of the component models to be close to the observed values as part of their initialization and spin up procedure, and recognizing that the overwhelming majority of water within the simulated system is in the ocean. Here seawater has global volume-mean values of 0.05‰ and 0.4‰ for δ18O and δD, respectively.

Despite the goal of mass conservation, after coupling all the components together, there is a drift in the total water isotopes in the ocean. The trend in global volume-averaged $\delta^{18}O$ in the ocean is about -0.05 ‰ kyr^{-1}. Further diagnostics suggest that the drift is attributable primarily to the isotope-enabled atmosphere and secondly to the land model. To mitigate this drift, an optional flux correction can be implemented at the ocean surface, adding a constant isotope water flux to compensate for the lost isotopic water. This optional flux correction removes trend in global mean ocean $\delta^{18}O$ and δD. After more than 1000 years of integration with the flux correction, trend in surface ocean $\delta^{18}O$ is on the order of -0.001‰ kyr^{-1}, which reflects the internal adjustments of $\delta^{18}O$ within the ocean. If long simulations (~1000 model years) are required, we recommend that this flux correction be turned on, as the numerical drift in $\delta^{18}O$ could be significant, particularly in the upper ocean. Note that a comparable drift in water isotopes has been reported from other modeling groups (e.g., Russon et al. 2013).

3. Results

3.1 Transient Last Millennium simulation

The simulation analyzed here is the 20th century portion of a transient simulation of the last millennium, covering 850–2005CE. This simulation was run using the same configuration (model resolution and transient external forcings) as the CESM Last Millennium Ensemble (LME; Otto-Bliesner et al. 2016), including time-varying orbital configurations, solar irradiances, and greenhouse gas emissions, as well as volcanic aerosol forcing and anthropogenic influences from aerosol emissions and land-use/land cover changes.

The Last Millennium iCESM simulation was initialized from a pre-industrial control simulation with fixed 850CE forcings, which was initialized from the gridded seawater $\delta^{18}O$ dataset of LeGrande and Schmidt (2006) and integrated for 1000 years to allow equilibration. Initial conditions for δD were generated by scaling $\delta^{18}O$ by a factor of 8. These initial conditions were chosen to minimize the computational cost of ocean spinup, which can take up to 6,000 years if initialized far from equilibrium (Jahn et al. 2015; Zhang et al. 2017). iCLM4 and iCAM5 were initialized from a near equilibrium state from a previous 150-year simulation with fixed SST. Uncoupled experiments suggest approximately 50 years is sufficient to bring deep soil water isotope ratios close to equilibrium in most locations. From this simulation, the transient last millennium run was branched off at year 850 and run with subsequent time-varying forcings as described above. This approach was also used to create other Last Millennium iCESM1 experiments, including both fully-forced (using all external forcing factors) and single-forcing experiments.

3.2 Atmospheric and terrestrial perspectives

The simulated physical state of the atmosphere in iCESM1 compares reasonably well to ERA-Interim, (Figures 2 and 3), although there are noticeable biases, such as the presence of a double-ITCZ. The model is also generally too cold and too humid relative to ERA-Interim, consistent with iCAM results from Nusbaumer et al. (2017). Figure 4 shows the average $\delta^{18}O$ of precipitation (4a) and d-excess of precipitation (4b), compared with the Global Network of isotopes in Precipitation (GNIP). As shown below, and known from observations, the spatial variation in isotope ratios in the ocean are quite small relative to variations in precipitation. Therefore, differences in the simulations of isotope ratios in iCESM relative to iCAM result mainly from differences in the simulation of the climate when ocean temperatures are allowed to evolved rather than using observed SSTs. Consequently, the broad features, also simulated in the uncoupled configuration, are reproduced here: polar regions have low isotope ratios due to systematic rainout during transport, the subtropical regions have high delta values associated with regions where evaporation dominates, the ITCZ region is a local minimum, and continental interiors have generally lower isotope ratios than surrounding oceans (viz., Dansgaard, 1964). As in the uncoupled model, the residence time for water in the atmosphere is on the order of weeks-to-months, and therefore these isotope relationships emerge from the simulation and are free from the influence

of the initial state after the spin up period. Figures 4c and 4d show a scatter plot of the iCESM1 precipitation $\delta^{18}O$ (4c) and d-excess (4d) values for the grid-points closest to the GNIP stations, with the black solid line representing a perfect match. iCESM1 captures the general qualitative and quantitative features of isotopes in precipitation, but does exhibit a depleted bias in precipitation $\delta^{18}O$ (median bias = − 2.5 ‰), which is comparable to that in the uncoupled configuration (median bias = − 2.2 ‰ from Nusbaumer et al. 2017). The deuterium excess, d-excess (defined d-excess = $\delta D - 8*\delta^{18}O$) values are not simulated well, with less correlation with the observations and too large a mean (median bias = 3.3 ‰). The magnitude of this bias is similar to that found in previous works with prescribed ocean and sea ice values (Nusbaumer et al. 2017; Wong et al. 2017). This implies that these particular biases are products of the atmosphere and land-surface components alone. However, differences between iCESM and iCAM5.3 do exist, for example, the precipitation $\delta^{18}O$ (Figure 4e) and d-excess (Figure 4f). Relatively large differences exist over Africa, Antarctica, and the central United States, although these regions have relatively few GNIP observations, which it makes it difficult to validate these differences quantitatively.

Figure 5 shows the differences in surface (lowest model level) air temperature, precipitable water, and evaporation minus precipitation for the two different models. It can be seen that many of the isotopic differences may be explained by differences in climate, such as higher temperatures over Antarctica in iCESM1, along with a dryer, more evaporative climate in the Caribbean/Central America. However, some isotopic differences, such as the large isotopic differences over Africa, do not seem to be as well explained by differences in the local climate alone, and warrant further study. A more detailed discussion of these general biases can be found in (Nusbaumer et al. 2017; Wong et al. 2017; Risi et al. 2010; Werner et al. 2011; Werner et al. 2016).

For many paleoclimate applications the relationship between isotope ratios and other climate parameters is important. Figure 6 shows a scatter-plot of the time-averaged values of precipitation $\delta^{18}O$ versus δD of precipitation (Figure 6a), surface air temperature versus precipitation $\delta^{18}O$ (5b), and precipitation rate versus precipitation $\delta^{18}O$ (6c) for both the GNIP data (blue) and the iCESM grid-cells closest to the GNIP station locations (red). Figure 6b only uses stations poleward of 45° N/S, whereas Figure 6c only uses stations equatorward of 25° N/S. The solid lines represent the linear regression between the respective scatter-plot quantities for both the observations and the model. The slopes of those regression lines are displayed on each plot as well.

It can be seen that the Global Meteoric Water Line (GMWL) (Craig, 1961), or the regression between $\delta^{18}O$ and δD, is well simulated by iCESM1, although the depleted bias can be seen in the δD values themselves. This agreement of modeled GMWL is due to the simulation of isotopic hydrological cycle in the atmosphere and land and is found to be independent of initial conditions in the ocean. The air-temperature versus $\delta^{18}O$ slope is too shallow in iCESM1, which is associated with the fact that the model is too depleted in the tropics and extratropics relative to observations, but then becomes too enriched at high latitudes. This is particularly true for loca-

tions with annual average temperatures less than 5° C, where the iCESM1 slope is substantially shallower than the GNIP observations (not shown). This overly-shallow slope in iCESM1 appears larger than was the case in iCAM3 (Guan et al. 2016), and may be related to biases in extratropical moisture transport in iCAM5, as discussed in Nusbaumer et al. (2017). Further, the precipitation rate versus $\delta^{18}O$ slope, which can be thought of as representing the "amount effect" (Dansgaard, 1964), is too strong in iCESM1 relative to observations (Figure 6c). While a complete theory to describe the mechanisms leading to the amount effect remains elusive, parameterized cloud and precipitation processes are likely partly responsible. For instance, the shortcoming could potentially be due to the model parameterization for isotopic fractionation during rain evaporation, which has previously been identified as a leading (and tunable) control on deuterium excess over land (e.g., Jouzel et al., 1987, Hoffmann et al., 1998, Noone and Simmonds, 2002; Bony et al., 2008). Finally, it was found that all of these regression relationships and biases hold for specific seasons as well (not shown), implying that the correlations are not just a seasonal-cycle effect, but are instead the result of multi-timescale relationships present in both the observations and model simulation.

3.3 Ocean and sea ice perspectives

The biases of SST and sea surface salinity (SSS) against the WOA13v2 observational climatology (Boyer et al. 2013) for the modern (1955–2005) portion of the last millennium run in iCESM1 are shown in Figure 7. The performance of iCESM is comparable to the non-isotope-enabled configuration (Otto-Bliesner et al. 2016). The large warm SST biases that originate in upwelling regions along the west coasts of continents and extend into the open ocean in CCSM4 (Danabasoglu et al. 2012) have been greatly reduced in iCESM1. The biases are less extensive spatially and limited to regions that are immediately adjacent to the coasts. In addition, the cold SST biases over the Southern Ocean in CCSM4 are not present in iCESM1. SSS in iCESM1 shows an overall fresh bias, similar to previous CCSM versions (Danabasoglu et al. 2012).

The model simulated $\delta^{18}O$ of surface water is compared with the climatological surface data of Global Seawater Oxygen-18 (GISS-O18) Database v1.21 (LeGrande & Schmidt 2006, Bigg and Rohling, 1999; accessible at: http://data.giss.nasa.gov/o18data/) in Figure 8. iCESM1 captures the major features in observations, including the relatively enriched water (~0.5–1 ‰) in the subtropics, the depleted water (< −1‰) in the Arctic, and the inter-basin contrast in $\delta^{18}O$ between the Atlantic and Pacific Ocean. These features largely reflect moisture transport in the atmosphere. Net evaporation occurs in the subtropical oceans, preferentially removing the lighter ^{16}O and resulting in ^{18}O-enriched seawater there. After evaporation, the atmospheric circulation transports the ^{18}O-depleted vapor to high latitudes and forms precipitation, decreasing the seawater $\delta^{18}O$ where the precipitation deposits. Similarly, along the ITCZ, high precipitation rates give rise to locally low δD and $\delta^{18}O$ values (i.e., contrast 8b with 2a and 4a). Overall, there is a net moisture transport from the Atlantic to the Pacific, which is also consistent with the more ^{18}O-enriched seawater in the Atlantic. iCESM1 captures these major features quite well; the model correctly produces local $\delta^{18}O$ maxima in the centers of the Pacific subtropical gyres and

the larger mean $\delta^{18}O$ in the Atlantic relative to the Pacific. The overall negative bias in seawater $\delta^{18}O$ is consistent with the fresh bias in salinity, suggesting a common cause in simulating the hydrological cycle (Danabasoglu et al. 2012). $\delta^{18}O$ over the Maritime Continent is more negative than predicted by LeGrande & Schmidt (2006); this discrepancy is likely due to a combination of the limited data availability in the region and the strong influences of precipitation and river runoff, which may not be well simulated by iCESM1.

To evaluate the simulation of subsurface $\delta^{18}O$ and related water mass signatures, zonal mean $\delta^{18}O$ in the Pacific and Atlantic is compared against the gridded GISS data set (LeGrande and Schmidt, 2006) in Figure 9. iCESM1 reproduces the $\delta^{18}O$ signature of major water masses, such as the North Atlantic Deep Water values of ~0.2–0.4 ‰ (Figure 9d) and the slightly negative Antarctic Bottom Water and Antarctic Intermediate Water (Figures 9c,d). One deficiency of the current simulation is that the upper ocean in the tropics and subtropics is too depleted in ^{18}O when compared with observations, in both the Atlantic and Pacific. Given the similar fresh bias in salinity over these regions (Danabasoglu et al. 2012; Figure 7), we argue that biases in seawater $\delta^{18}O$ and salinity may originate from common biases in simulating the bulk hydrological cycle and/or ocean dynamics, instead of isotopic processes. This could arise, for instance, due to errors in the simulated location of the jet and therefore gyre extent, or in the degree of deep water formation. We also note that model spinup should not play a significant role in generating model-data offsets, since the simulation has been integrated over 1,500 years since initialization; the solution thus likely reflects mainly the physical processes resolved in the model.

Another key metric of oceanic isotopic performance is the relationship between salinity and the $\delta^{18}O$ of seawater (Figure 10). The two variables are known to covary substantially (LeGrande & Schmidt 2006; Conroy et al. 2015), and $\delta^{18}O$ is therefore often considered to be a proxy for salinity (e.g. Thompson et al. 2011). The ability of iCESM1 to capture the relationship between the two variables is evaluated in Figure 10, by subsampling iCESM1 output at the nearest gridpoint to each GISS database entry over the appropriate month and year. iCESM1 is generally able to well capture the salinity:$\delta^{18}O$ relationship in both the Atlantic and Pacific, although the slope appears systematically shallower in iCESM in most regions. Mismatches in slope are largest in the North Pacific, which could arise from issues with the simulation of storm track dynamics as noted above. Some of these mismatches may also arise from undersampling of internal variability in observations, as noted by Stevenson et al. (2018). Additionally, there is a systematic trend towards weaker slopes with time in the North Atlantic salinity:$\delta^{18}O$ relationship; the causes for this trend are unclear, but may represent an influence from anthropogenically driven climate changes.

3.4. Coupled applications

Coupled isotope-enabled simulations are crucial tools in many areas of paleoclimate studies, both for benchmarking climate models and investigating fundamental questions in climate dynamics. This is particularly obvious in cases where the objective is to understand the response

of modes of coupled climate variability to external forcing, which requires a coupled modeling framework in order to properly evaluate the dynamics responsible for generating signals observed in the paleoclimate record. Examples of such studies include the response of ENSO to external forcings (e.g. volcanic, solar, GHGs, ice sheets, meltwater; Mann et al. 2005, Meehl et al. 2006; Anchukaitis et al. 2010; Liu et al. 2014a; Stevenson et al. 2016; Zhu et al. 2017a), abrupt climate changes and role of the Atlantic Meridional Overturning Circulation (e.g. Liu et al. 2009; Otto-Bliesner and Brady, 2010, Bakker et al. 2016), the response of monsoons and hydroclimate to climate forcings (e.g. Otto-Bliesner et al. 2014; Liu et al. 2014b), and the role of changing orbital configurations in altering the expression of these and other modes of variability (e.g. Karamperidou et al. 2015; Lu and Liu, 2018). Here we present analyses demonstrating the value of the coupled configuration of iCESM1 for both modern and paleoclimate applications.

The isotopic expression of the El Nino/Southern Oscillation (ENSO) in iCESM1 is shown in Figure 11; the regression patterns of precipitation amount (contours) and $\delta^{18}O$ of precipitation (colors) on the NINO3.4 index (5°S–5°N, 120–170°W average SST) are quite different. The model shows similar spatial pattern to previous forced atmospheric simulations (e.g., Hoffman et al. 1998, Noone and Simmonds 2002a) and within the SWING2 archive (Conroy et al. 2013). Distinctions between precipitation and its isotopic composition are particularly apparent in the subtropics and higher latitudes, where precipitation $\delta^{18}O$ exhibits substantial ENSO-induced variability in the near-absence of changes in precipitation amount (consistent with previous work, e.g., Moerman et al. 2013; Hurley et al. 2019). The dynamics of these effects have yet to be investigated fully, but it is known that moisture transport linked to ENSO involves coupling between the midlatitude and convective circulation, which can alter precipitation $\delta^{18}O$ through shifts in storm tracks and moisture transport pathways (e.g., Noone and Simmonds 2002b; Noone 2008; Vachon et al 2010).

Although ocean dynamics may play a role in generating the precipitation $\delta^{18}O$ patterns of Figure 11, the role of the coupled configuration is more obvious when examining the variations in seawater $\delta^{18}O$. Understanding the ENSO influence on seawater $\delta^{18}O$ is crucial to interpreting recent increases in $\delta^{18}O$ variance observed in the coral record in the late 20th century relative to the Holocene (Cobb et al. 2013), as both temperature and seawater $\delta^{18}O$ are known to influence coral $\delta^{18}O$ in the tropical Pacific. Additionally, recent work using isotope-enabled ocean models has demonstrated the capacity for ENSO-related seawater $\delta^{18}O$ to vary on decadal timescales (Stevenson et al. 2018). However, the dynamical controls on seawater $\delta^{18}O$ remain poorly understood, as do their potential responses to anthropogenic forcing – addressing both of these questions necessarily requires coupled simulations. As does precipitation $\delta^{18}O$, seawater $\delta^{18}O$ varies as a function of ENSO phase – the regression of seawater $\delta^{18}O$ on the NINO3.4 index is shown in Figure 11b. El Nino events are associated with enriched seawater $\delta^{18}O$ over the Maritime Continent and depleted seawater $\delta^{18}O$ in the western Pacific warm pool, and the patterns of seawater and precipitation $\delta^{18}O$ over the tropical Pacific bear a qualitative resemblance to one another (cf. Fig 11a vs. 11b). Figure 11c provides further insight, by depicting the regression of local sea-

water $\delta^{18}O$ on precipitation $\delta^{18}O$ anomalies. Over some portions of the tropical oceans, the sensitivity of seawater $\delta^{18}O$ to precipitation $\delta^{18}O$ is relatively small, likely indicating a dominant role for ocean dynamical processes in generating seawater $\delta^{18}O$ variations (Stevenson et al. 2018). However, under the climatological locations of the Intertropical and South Pacific Convergence Zones, the sensitivity is much larger, suggesting that the seawater $\delta^{18}O$ anomalies mentioned above are in fact driven in part by variations in precipitation $\delta^{18}O$. And of course, this result could not have been obtained without the use of a coupled, isotope-enabled modeling framework.

Isotope-enabled coupled simulations are also vital in other paleoclimate contexts. One example is on the interpretation of terrestrial $\delta^{18}O$ signal during Heinrich events, which are abrupt climate changes typically identified by ice-rafted debris deposits in high-latitude ocean sediments and are thought to be associated with collapse of North Atlantic ice sheets and associated increases in the discharge of icebergs into the region (Heinrich, 1988). Heinrich events are generally associated with minimum in $\delta^{18}O$ in Greenland ice cores, decreases in North Atlantic salinity associated with enhanced freshwater flux, and weakening of the Asian monsoon reflected in low-latitude speleothem records (e.g., Bond et al. 1993; Wang et al. 2001). However, the lack of a quantitative interpretation of signal in proxy archives is a primary barrier to a mechanistic understanding of Heinrich events and their global impacts. Recent work with the coupled iCESM1 has attempted to quantitatively interpret terrestrial $\delta^{18}O$ signals by directly comparing them with $\delta^{18}O$ anomalies in 'water hosing' experiments, i.e., injecting isotopically depleted meltwater with a $\delta^{18}O$ signature of –30 ‰ into the northern North Atlantic in iCESM1 (Zhu et al. 2017b). Figure 12 shows that the magnitude and spatial features of speleothem $\delta^{18}O$ changes during Heinrich events can be well-reproduced using iCESM1. Additionally, iCESM1 can be used to quantify the roles of the 'direct meltwater effect' (a non-climatic influence from the ^{18}O-depleted signature of the meltwater) versus the climatic effects resulted from freshwater forcing. This was accomplished by Zhu et al. (2017b) via sensitivity experiments with injection of a non-depleted meltwater with a $\delta^{18}O$ signature of 0 ‰. Results suggest that a large portion of the $\delta^{18}O$ variations (e.g., 15–35% over eastern Brazil; see Figure 1 in Zhu et al. 2017b) can be related to the direct meltwater effect (a non-climatic effect) from the depleted meltwater, instead of changes in monsoon intensities. This indicates that physical process-based modeling of water isotopes is critical. Additionally, combining iCESM with proxy records can help constrain other physical processes which are poorly understood during Heinrich events, e.g., the magnitude and location of freshwater discharge (Roche et al. 2014; Zhu et al. 2017b).

4. Discussion and Conclusions

The isotope-enabled version of the Community Earth System Model, iCESM1 has been presented. Water isotope ratios are directly simulated within all components of iCESM1, with communication between the atmosphere (CAM5.3), land (CLM4), sea ice (CICE4), and ocean

(POP2) components. Isotope ratios are simulated via the inclusion of a tracer hydrologic cycle that follows "standard" model water through all relevant flux exchanges, with both kinetic and equilibrium fractionation applied during phase change, and from which the hydrological balance emerges in a fully consistent framework. In the coupled configuration, there is the option for a 'flux correction' to prevent long-term (multi-centennial) isotopic drift, which is relevant primarily for long paleoclimate simulations.

The simulation of physical variables in iCESM1 is essentially identical to the underlying, non-isotope-enabled released version of CESM1 with the exception of minor code updates, and the fidelity of the iCESM1 simulation thus follows closely the performance of released CESM1 (Hurrell et al. 2013, Kay et al. 2014, Otto-Bliesner et al. 2016, Danabasoglu et al. 2011). iCESM1 is shown to capture the broad qualitative features of precipitation isotopic patterns, albeit with a low bias in $\delta^{18}O$ values of precipitation. The representation of $\delta^{18}O$ is more accurate than that of d-excess, whose values are too low over land and do not correlate as well with observations, consistent with stand-alone simulations in iCAM5 and iCLM4 (Nusbaumer et al. 2017, Wong et al. 2017). This result highlights the importance of continued refinement of the simulated hydrological cycle associated with clouds and terrestrial processes. On the other hand, the isotopic simulation of precipitation has only weak dependence on the evolving isotope ratios of sea water. Of importance for paleoclimate applications, the relationship between temperature, precipitation, and precipitation $\delta^{18}O$ are reproduced in CESM but also reflect iCAM5; the temperature/$\delta^{18}O$ slope is too shallow and the precipitation amount/$\delta^{18}O$ slope too steep compared with observations. The fact that iCAM5 and iCLM4 closely follow the modeling structure of the base CAM5 and CLM4 models means that biases in the isotopic model versions offers unique opportunities to detect and improve shortcomings in the base models.

iCESM1 well captures the geographic structure of seawater $\delta^{18}O$, including subtropical enrichment, Arctic depletion, and inter-basin contrasts between the Atlantic and Pacific; these features are related to the structure of moisture transport in the atmosphere. The isotopic signatures of major water masses are also well captured by iCESM1, although the tropical/subtropical upper ocean appears to be depleted in ^{18}O relative to observations. This likely relates to issues with simulating the bulk hydrological cycle and/or ocean dynamics, since isotopic biases closely track biases in salinity (Danabasoglu et al. 2012). The relationship between salinity and seawater $\delta^{18}O$, a parameter of key interests for paleoclimate applications, is also well captured by iCESM1.

Interpretation of isotopic measurements from the calcium carbonate of speleothems is one useful application of the coupled iCESM1 (Liu et al. 2014b; Tabor et al. 2018). While iCESM1 cannot directly simulate the cave drip water that ultimately produces the speleothem records, the simulated transport of water isotopes through the land and atmosphere provide several signals for comparison with the proxy records. Furthermore, outputs from iCESM1 can be added into forward proxy models to provide valuable insights into how seasonal and annual isotopic variability translate into the speleothem records (e.g. Dee et al. 2015). Previous work has

already shown the utility of this approach in constraining the properties of Heinrich events (Zhu et al. 2017b), glacial ENSO variability (Zhu et al. 2017a), and orbital-scale monsoon variability (Tabor et al. 2018), and we anticipate that future investigations with iCESM over a wide variety of time periods will yield similar advances.

iCESM code is publicly accessible via Github (https://github.com/NCAR/iCESM1.2).

Acknowledgements

This material is based upon work supported by the National Center for Atmospheric Research, which is a major facility sponsored by the National Science Foundation under Cooperative Agreement No. 1852977. Additional funding to ECB and BO-B was provided by an NSF P2C2 grant (AGS-1401803). JN was supported by the NASA Post-doctoral Program (NPP) fellowship. SS was supported by an NSF P2C2 grant (AGS-1805143), and an NSF EaSM grant (AGS-1243125). ZL, JZhang and JZhu were supported by an NSF P2C2 grant (AGS-1810682). JZhang acknowledges Regional and Global Climate Modeling Program of the U.S. DOE through support of the HiLAT project and CNLS sponsored by LDRD. DN acknowledges support from the NSF P2C2 and Climate and Large-scale Dynamics programs (AGS-1502806, AGS-1049104, AGS-0955841 and AGS-1564670) The CESM project is supported primarily by the National Science Foundation. Computing resources (*doi:10.5065/D6RX99HX*) were provided by the Climate Simulation Laboratory at NCAR's Computational and Information Systems Laboratory, sponsored by the National Science Foundation and other agencies.

References

Aggarwal , P. K., U. Romatschke, L. Araguas-Araguas, D. Belachew, F. J. Longstaffe, P. Berf, C. Schumacher, and A. Funk, Proportions of Convective and Stratiform Precipitation Revealed in Water Isotope Ratios, *Nature Geoscience*, 9, 624-629, 2016.

Anchukaitis, K.J. and M.N. Evans, Tropical cloud forest climate variability and the demise of the Monteverde Golden Toad, *Proceedings of the National Academy of Sciences*, 107(11), 5036-5040, doi:10.1073/pnas.0908572107, 2010.

Bagniewski, W., K. J. Meissner, L. Menviel, and C. E. Brennan, Quantification of factors impacting seawater and calcite d18O during Heinrich Stadials 1 and 4, *Paleoceanography*, *30*(7), 895–911, 2015.

Bakker, P., et al., Fate of the Atlantic Meridional Overturning Circulation: Strong decline under continued warming and Greenland melting, Geophys. Res. Lett., 43, 12,252–12,260, 2016, doi:10.1002/ 2016GL070457.

Bellenger H, E. Guilyardi, J. Leloup, M. Lengaigne, and J. Vialard, ENSO representation in climate models: from CMIP3 to CMIP5, *Climate Dynamics*, 2014, doi:10.1007/s00382-013-1783-z

Berkelhammer, M., C. Risi, N. Kurita, and D. C. Noone, The moisture source sequence for the Madden-Julian Oscillation as derived from satellite retrievals of HDO and H2O, *J. Geophys. Res*., 117, D03106, 2012, doi:10.1029/2011JD016803.

Bond, G., Broecker, W., Johnsen, S., McManus, J., Labeyrie, L., Jouzel, J., & Bonani, G. (1993). Correlations between climate records from North Atlantic sediments and Greenland ice. Nature, 365(6442), 143–147.

Boyer, T.P., J. I. Antonov, O. K. Baranova, C. Coleman, H. E. Garcia, A. Grodsky, D. R. Johnson, R. A. Locarnini, A. V. Mishonov, T.D. O'Brien, C.R. Paver, J.R. Reagan, D. Seidov, I. V. Smolyar, and M. M. Zweng, World Ocean Database 2013, NOAA Atlas NESDIS 72, S. Levitus, Ed., A. Mishonov, Technical Ed.; Silver Spring, MD, 209 pp., 2013, http://doi.org/10.7289/V5NZ85MT

Buenning, N., D. Noone, W. Riley, C. Still and J White, Influences of the hydrological cycle on observed inter-annual variations in atmospheric $CO^{18}O$, *Journal of Geophysical Research-Biogeoscience*. **116**, G04001, 2011, doi:10.1029/2010JG001576.

Caley, T., and D. Roche, d18O water isotope in the iLOVECLIM model (version 1.0)–Part 3: A palaeo-perspective based on present-day data–model comparison for oxygen stable isotopes in carbonates, *Geoscientific Model Development*, *6*(5), 1505–1516, 2013.

Conroy, J., K. M. Cobb, and D. Noone, Comparison of precipitation isotope variability across the tropical Pacific in observations and SWING2 model simulations, *Journal of Geophysical Research – Atmospheres*. 118(11), 5867-5892, 2013, doi: 10.1002/jgrd.50412.

Craig, H, Isotopic Variations in Meteoric Waters. *Science*. 133, Issue 3465, 1702-1703, 1961, doi: 10.1126/science.133.3465.1702.

Craig, H., and L. Gordon, Deuterium and oxygen-18 in the ocean and the marine atmosphere, in Stable Isotopes in Oceanographic Studies and Paleotemperatures, edited by E. Tongiorgi, pp. 9-130, Spoleto, 1965.

Danabasoglu, G., S. C. Bates, B. P. Briegleb, S. R. Jayne, M. Jochum, W. G. Large, S. Peacock, and S. G. Yeager, The CCSM4 Ocean Component. J. Clim., 25, 1361–1389, 2011, doi:10.1175/JCLI-D-11-00091.1.

Danabasoglu, G., Bates, S. C., Briegleb, B. P., Jayne, S. R., Jochum, M., Large, W. G., ... & Yeager, S. G. (2012). The CCSM4 ocean component. Journal of Climate, 25(5), 1361-1389.

Dansgaard, W, Stable isotopes in precipitation. *Tellus*. **16**, Issue 4, 436-468, 1964, doi: 10.1111/j.2153-3490.1964.tb00181.x.

Delaygue, G., J. Jouzel, and J.-C. Dutay, Oxygen 18–salinity relationship simulated by an oceanic general circulation model, *Earth and Planetary Science Letters*, *178*(1), 113–123, 2000**.**

Dee, S., D. Noone, N. Buenning, J. Emile-Geay, and Y. Zhou, SPEEDY-IER: A fast atmospheric GCM with water isotope physics. *Journal of Geophysical Research – Atmospheres*, **120**(1), 73-91, 2015, doi: 10.1002/2014JD022194.

Dee S.G., J. Nusbaumer, A. Bailey, J.M. Russell, J.-E. Lee, B.L Konecky, N. Buenning, and D. Noone, Tracking the Strength of the Walker Circulation with Stable Isotopes in Water Vapor, J. Geophys. Res. Atmos., 123, 2018 https://doi.org/10.1029/2017JD027915

Dominguez, F., G. Miguez-Macho, and H. Hu, WRF with Water Vapor Tracers: A Study of Moisture Sources for the North American Monsoon. *Journal of Hydrometeorology*. **17**, 1915-1927, 2016, doi: 10.1175/JHM-D-15-0221.1.

Dyer, E. L. E., Jones, D. B. A., Nusbaumer, J., Li, H., Collins, O., Vettoretti, G., and D. Noone, Congo Basin precipitation: Assessing seasonality, regional interactions, and sources of moisture. *Journal of Geophysical Research - Atmospheres*. **122**, Issue 13, 6882-6898, 2017, doi: 10.1002/2016JD026240.

Field, R. D., D. Kim, A. N. LeGrande, J. Worden, M. Kelley, and G. A. Schmidt (2014). Evaluating climate model performance in the tropics with retrievals of water isotopic composition from Aura TES. *Geophysical Research Letters*. **41**(16), 6030-6036, doi: 10.1002/2014GL060572.

Galewsky, J., H. C. Steen-Larsen, R. D. Field, J. Worden, C. Risi, and M. Schneider (2016), Stable isotopes in atmospheric water vapor and applications to the hydrologic cycle. *Reviews of Geophysics*. **54**, Issue 4, 809-865, doi: 10.1002/2015RG000512.

Gat, J.R. (1996), Oxygen and hydrogen isotopes in the hydrologic cycle, *Annual Review of Earth and Planetary Sciences*, 24, 225-262.

Gat, J.R., (2000) Atmospheric water balance- the isotopic perspective. *Hydrological Processes* 14, 1 357- 1369.

Grootes, P. M., Stuiver, M., White, J. W. C., Johnsen, S., & Jouzel, J. (1993). Comparison of oxygen isotope records from the GISP2 and GRIP Greenland ice cores. Nature, 366(6455), 552–554. https://doi.org/10.1038/366552a0

Guan, J., Z. Liu, X. Wen, E. Brady, D. Noone, J. Zhu, and J. Han, 2016: Understanding the temporal slope of the temperature-water isotope relation during the deglaciation using isoCAM3: The slope equation, *J. Geophys. Res. Atmos*., 121, doi:10.1002/2016JD024955.

Heinrich, H. (1988). Origin and Consequences of Cyclic Ice Rafting in the Northeast Atlantic Ocean During the Past 130,000 Years. Quaternary Research, 29(2), 142–152.

Hoffmann, G., M. Werner, and M. Heimann (1998). Water isotope module of the ECHAM atmospheric general circulation model: A study on timescales from days to several years. *Journal of Geophysical Research - Atmospheres*, **103**(16), doi: 10.1029/98JD00423.

Hurrell, J. W., and Coauthors (2013). The Community Earth System Model: A Framework for Collaborative Research. *Bulletin of the American Meteorological Society*. **94**(9), 1339-1360, doi: 10.1175/BAMS-D-12-00121.1.

Hu J., Emile-Geay, J., Nusbaumer, J., & Noone, D. (2018). Impact of convective activity on precipitation δ18O in isotope-enabled general circulation models. *Journal of Geophysical Research: Atmospheres*, 123, 13,595–13,610. https://doi.org/10.1029/2018JD029187

Hunke, E. C. and Lipscomb, W. H. (2010). CICE: the Los Alamos Sea Ice Model Documentation and Software User's Manual Version 4.1. Tech. Rep., Los Alamos National Laboratory Tech. Rep. LA-CC-06-012.

IAEA/WMO (2016), *Global Network of Isotopes in Precipitation (GNIP)*, Vienna, Austria, available at http://www-naweb.iaea.org/napc/ih/IHS_resources_gnip.html.

Jahn, A., K. Lindsay, X. Giraud, N. Gruber, B. L. Otto-Bliesner, Z. Liu, and **E. C. Brady**, Carbon isotopes in the ocean model of the Community Earth System Model (CESM), *Geosci. Model Dev*, 8, 2419-2434, DOI: 10.5194/gmd-8-2419-2015.

Joussaume, S.,J. Jouzel and R. Sadourny, 1984: A general circulation model of water isotope cycles in the atmosphere. Nature, 311, 24-29

Jouzel, J. and Merlivat, L. (1984). Deuterium and oxygen 18 in precipitation: Modeling of the isotopic effects during snow formation. *Journal of Geophysical Research 89: doi: 10.1029/JD089iD07p11749. issn: 0148-0227.*

Jouzel, J., G. Russell, R. Suozzo, R. Koster, J. White, andW. Broecker, Simulations of the HDO and $H_2{}^{18}O$ atmospheric cycles using the NASA GISS general circulation model: The seasonal cycle for present-day conditions, Journal of Geophysical Research, 92(14), 739–14, 1987.

Jouzel, J., R. Koster, R. Suozzo, G. Russell, J. White, and W. Broecker, Simulations of the HDO and H2 180 atmospheric cycles using the NASA GISS general circulation model: Sensitivity experiments for present-day conditions, J. Geophys. Res., 96, 7495-7507, 1991.

Kanner, L, N. Buenning, L. Stott, A. Timmermann and D. Noone, 2014: The role of soil processes in d18O terrestrial climate proxies. *Global Biogeochemical Cycles*,28, 239.252, doi:10.1002/2013GB004742.

Karamperidou, C., DiNezio, P. N., Timmermann, A., Jin, F.-F. and Cobb, K. M. (2015): The response of ENSO flavors to mid-Holocene climate: Implications for proxy interpretation. *Paleoceanography and Paleoclimatology*, 30 (5), 527-547.

Konecky, B. L., Russell, J. M., Rodysill, J. R., Vuille, M., Bijaksana, S. and Huang, Y. (2013): Intensification of southwestern Indonesian rainfall over the past millennium. *Geophysical Research Letters*, 40, 386-391, doi:10.1029/2012GL054331.

Konecky, B. L., Noone, D. C., & Cobb, K. M. (2019). The influence of competing hydroclimate processes on stable isotope ratios in tropical rainfall. Geophysical Research Letters, 46.

Kopec, B. G., X. Feng, F. A. Michel, and E. S. Posmentier (2016), Influence of sea ice on Arctic precipitation, Proc. Natl. Acad. Sci. U.S.A., 113(1), 46–51, doi:10.1073/pnas.1504633113.

Koster, R., Jouzel, J., Suozzo, R., Russell, G., Broecker, W., Rind, D., and P. Eagleson (1986). Global sources of local precipitation as determined by the Nasa/Giss GCM. *Geophysical Research Letters*. 13(2), 121-124, doi: 10.1029/GL013i002p00121.

Kuang, Z., G. C. Toon, P. O. Wennberg, and Y. L. Yung (2003), Measured HDO/H2O ratios across the tropical tropopause, Geophys. Res. Lett., 30(7), 1372, doi:10.1029/2003GL017023.

LeGrande, A. N. and G. A. Schmidt, 2006: Global gridded data set of the oxy- gen isotopic composition in seawater. Geophysical Research Letters, 33, L12604, doi: 10.1029/2006GL026011.

LeGrande, A. N., and G. A. Schmidt, Ensemble, water isotope–enabled, coupled general circulation modeling insights into the 8.2 ka event, *Paleoceanography*, 23(3), 2008.

Lehmann, M, and U Siegenthaler. 1991. Equilibriunl oxygen-and hydrogen-isotope fractionation between ice and water. J. Glaciol. 37(125):23–26.

Lewis, S. C., LeGrande, A. N., Kelley, M., and G. A. Schmidt (2010). Water vapour source impacts on oxygen isotope variability in tropical precipitation during Heinrich events. *Climate of the Past*. **6**, 325-343, doi: 10.5194/cp-6-325-2010.

Liu, Z., B. Otto-Bliesner, F. He, E. Brady, P. Clark, J. Lynch-Steiglitz, A. Carlson, W. Curry, E. Brook, R. Jacob, D. Erickson, J. Kutzbach, J. Cheng, 2009: Transient simulation of deglacial Climate Evolution with a new mechanism for Bolling-Allerod warming. Science, 325, 310-314.

Liu, Z., X. Wen, E. Brady, B. Otto-Bliesner, G. Yu, H. Lu, H. Cheng, Y. Wang, W. Zheng, Y. Ding, L. Edwards, J. Cheng, W. Liu and H. Yang, 2014: Chinese cave records and East Asian Summer Monsoon. Quat. Sci. Rev., 83, 115–128.

Liu Z., Z. Lu, X. Wen, B. Otto-Bliesner, A. Timmermann, K. Cobb, 2014: The evolution and forcing mechanism of El Nino in the last 21,000 years. Nature, 515, 550-553

Lu, Z. and Z. Liu, 2018: Orbital modulation of ENSO seasonal phase locking. Clim. Dyn., DOI 10.1007/s00382-018-4382-1

Mathieu, R., D. Pollard, J. Cole, J. White, R. Webb, and S. Thompson, Simulation of stable water isotope variations by the GENESIS GCM for modern conditions, *Journal of Geophysical Research-Atmospheres*, *107*(D4), 4037, 2002.

Majoube, M., 1971: FRACTIONATING OF d18o BETWEEN ICE AND WATER VAPOR. J. Chim. Phys. Physico-Chimie Biol., 68, 625. Http://www.osti.gov/scitech/biblio/4019841.

Meehl, G.A., H. Teng, and G.W. Branstator, 2006: Future changes of El Nino in two global coupled climate models. *Cli. Dyn.*, 581-609.

Merlivat, L. and Jouzel, J. (1979) Global Climatic Interpretation of the Deuterium-Oxygen 18 Relationship for Precipitation. Journal of Geophysical Research, 84, 5029-5033. http://dx.doi.org/10.1029/JC084iC08p05029

Neale, R. B., Chen, C., Gettelman, A., Lauritzen, P. H., Park, S., Williamson, D. L., Conley, A. J., Garcia, R., Kinnison, D., Lamarque, J., Marsh, D., Mills, M., Smith, A. K., Tilmes, S., Vitt, F., Morrison, H., Cameron-Smith, P., Collins, W. D., Iacono, M. J., Easter, R. C., Ghan, S. J., Liu, X., Rasch, P. J., and M. A. Taylor (2010). Description of the NCAR Community Atmosphere Model (CAM 5.0). *NCAR Technical Note-Scientific and Technical Report, NCAR/TN-486+STR*.

NEEM community members (2013). Eemian interglacial reconstructed from a Greenland folded ice core. Nature, 493(7433), 489–494. https://doi.org/10.1038/nature11789

Noone, D., and I. Simmonds (2002). Annular variations in moisture transport mechanisms and the abundance of δ18O in Antarctic snow. *Journal of Geophysical Research - Atmospheres*. **107**, Issue D24, doi: 10.1029/2002JD002262.

Noone, D., 2008: The influence of midlatitude and tropical overturning circulation on the isotopic composition of atmospheric water vapor and Antarctic precipitation. *Journal of Geophysical Research,* **113**, D04102, doi:10.1029/2007JD008892.

Noone, D. (2012), Pairing measurements of the water vapor isotope ratio with humidity to deduce atmospheric moistening and dehydration in the tropical midtroposphere, J. Clim., 25, 4476–4494.

Nusbaumer, J., Wong, T., Bardeen, C., and D. Noone (2017). Evaluating hydrological processes in the Community Atmosphere Model, Version 5 (CAM5) using stable isotope ratios of water. *Journal of Advances in Modeling Earth Systems*. **9**, Issue 2, 949-977, doi: 10.1002/2016MS000839.

Nusbaumer, J., and D. Noone (2018). Numerical Evaluation of the Modern and Future Origins of Atmospheric River Moisture over the West Coast of the United States. *Journal of Geophysical Research - Atmospheres*. **123**, Issue 12, 6423-6442, doi: 10.1029/2017JD028081.

Oleson, K. W., D. M. Lawrence, G. B., Bonan, et al. 2010. Technical Description of version 4.0 of the Community Land Model (CLM). Boulder: National Center for Atmospheric Research.

Otto-Bliesner, B.L., and E.C. Brady, 2010: The sensitivity of the climate response to the magnitude and location of freshwater forcing: last glacial maximum experiments. Quaternary Science Reviews, 29, 56-73.

Paul, A., S. Mulitza, J. Pätzold, and T. Wolff, Simulation of oxygen isotopes in a global ocean model, in *Use of Proxies in Paleoceanography*, pp. 655–686, Springer, 1999.

Petit, J. R., and Coauthors, 1999: Climate and atmospheric history of the past 420,000 years from the Vostok ice core, Antarctica. Nature, 399, 429. http://dx.doi.org/10.1038/20859.

Risi, C., S. Bony, F. Vimeux, and J. Jouzel (2010). Water-stable isotopes in the LMDZ4 general circulation model: Model evaluation for present-day and past climates and applications to climatic interpretations of tropical isotopic records. *Journal of Geophysical Research – Atmospheres*. **115**(D12), doi: 10.1029/2009JD013255.

Risi, C., and Coauthors (2012). Process-evaluation of tropospheric humidity simulated by general circulation models using water vapor isotopologues: 1. Comparison between models and observations. *Journal of Geophysical Research – Atmospheres*. **117**(D5), doi: 10.1029/2011JD016621.

Roche, D., D. Paillard, A. Ganopolski, and G. Hoffmann, Oceanic oxygen-18 at the present day and LGM: equilibrium simulations with a coupled climate model of intermediate complexity, *Earth and Planetary Science Letters*, *218*(3), 317–330, 2004.

Roche, D. M.: 2013: δ18O water isotope in the iLOVECLIM model (version 1.0) – Part I: Implementation and verification, Geosci. Model Dev., 6, 1481–1491, doi:10.5194/gmd-6-1481-2013.

Roche, D., M and T. Caley, 2013: δ18O water isotope in the iLOVECLIM model (version 1.0) – Part II:Evaluation of model results against observed δ18O in water samples., Geosci. Model Dev., 6, 1493–1504, doi:10.5194/gmd-6-1493-2013.

Roche, D. M., Paillard, D., Caley, T., & Waelbroeck, C. (2014). LGM hosing approach to Heinrich Event 1: Results and perspectives from data-model integration using water isotopes. Quaternary Science Reviews, 106, 247–261. https://doi.org/10.1016/j.quascirev.2014.07.020

Russon, T., A. W. Tudhope, G. C. Hegerl, M. Collins, and J. Tindall, 2013: Inter-annual tropical Pacific climate variability in an isotope-enabled CGCM: Implications for interpreting coral stable oxygen isotope records of ENSO. Clim. Past, 9, 1543–1557, doi:10.5194/cp-9-1543-2013.

Schmidt, G.A., 1998: Oxygen-18 variations in a global ocean model. *Geophys. Res. Lett.*, **25**, 1201-1204, doi:10.1029/98GL50866.

Schmidt, G. A., Forward modeling of carbonate proxy data from planktonic foraminifera using oxygen isotope tracers in a global ocean model, *Paleoceanography*, *14*(4), 482–497, 1999.

Schmidt, G.A., G. R. Bigg and E. J. Rohling. 1999. "Global Seawater Oxygen-18 Database - v1.22" https://data.giss.nasa.gov/o18data/

Schmidt, G.A., G. Hoffmann, D.T. Shindell, and Y. Hu, 2005: Modelling atmospheric stable water isotopes and the potential for constraining cloud processes and stratosphere-troposphere water exchange. *J. Geophys. Res.*, 110, D21314, doi:10.1029/2005JD005790.

Schmidt, G. A., A. N. LeGrande, and G. Hoffmann (2007), Water isotope expressions of intrinsic and forced variability in a coupled ocean-atmosphere model, J. Geophys. Res., 112, D10103, doi:10.1029/ 2006JD007781.

Singh, H. A., Bitz, C. M., Nusbaumer, J., and D. C. Noone (2016). A mathematical framework for analysis of water tracers: Part 1: Development of theory and application to the preindustrial mean state. *Journal of Advances in Modeling Earth Systems*. **8**, 991-1013, doi: 10.1002/2016MS000649.

Smith, R., P. Jones, B. Briegleb, F. Bryan, G. Danabasoglu, J. Dennis, J. Dukowicz, C. Eden, B. Fox-Kemper, P. Gent, M. Hecht, S. Jayne, M. Jochum, W. Large, K. Lindsay, M. Maltrud, N. Norton, S. Peacock, M. Vertenstein, and S. Yeager. 2010. The Parallel Ocean Program (POP)

Reference Manual, Ocean Component of the Community Climate System Model (CCSM). Tech. Rep., Los Alamos National Laboratory Tech. Rep. LAUR-10-01853.

Sodemann, H., Wernli, H., and C. Schwierz (2009). Sources of water vapour contributing to the Elbe flood in August 2002—A tagging study in a mesoscale model. *Quarterly Journal of the Royal Meteorological Society*. **135**, 205-223, doi: 10.1002/qj.374.

Stevenson, S. (2012). Significant Changes to ENSO Strength and Impacts in the 21st Century: Results from CMIP5, *Geophysical Research Letters*, 39, L17703

Stevenson, S., A. Capotondi, J. Fasullo, B. Otto-Blisener (2016). Forced changes to twentieth century ENSO diversity in a last Millennium context, Clim. Dyn., DOI 10.1007/s00382-017-3573-5.

Tabor, C. R., Otto-Bliesner, B. L., Brady, E. C., Nusbaumer, J., Zhu, J., Erb, M. P., Wong, T. E., Liu, Z., and D. Noone (2018). Interpreting precession driven $\delta^{18}O$ variability in the South Asian monsoon region. *Journal of Geophysical Research – Atmospheres*, **123**, Issue 11, 5927-5946, doi: 10.1029/2018JD028424.

Thompson, D.M., T.R. Ault, M.N. Evans, J.E. Cole, and J. Emile-Geay, (2011). Comparison of observed and simulated tropical climate trends using a forward model of coral δ18O. Geophys. Res. Lett., 38, L14706, doi:10.1029/2011GL048224.

Tindall, J. C., P. J. Valdes, and L. C. Sime, 2009: Stable water isotopes in HadCM3: Isotopic signature of El Ni??o-Southern Oscillation and the tropical amount effect. J. Geophys. Res. Atmos., 114, D04111, doi:10.1029/2008JD010825.

Tharammal, T., A. Paul, U. Merkel, and D. Noone, 2013: Influence of LGM boundary conditions on the global water isotope distribution in an atmospheric general circulation model *Clim. Past*, 9, 789.809, doi:10.5194/cp-9-789-2013.

Toyota, T., I. J. Smith, A. J. Gough, P. J. Langhorne, G. H. Leonard, R. J. Van Hale, A. R. Mahoney, and T. G. Haskell, 2013: Oxygen isotope fractionation during the freezing of sea water. J. Glaciol., 59, 697–710, doi:10.3189/2013JoG12J163.

Tremoy, G., F. Vimeux, S. Soumana, I. Souley, C. Risi, G. Favreau, and M. Oi(2014), Clustering mesoscale convective systems with laser-based water vapor delta O-18 monitoring in Niamey (Niger), J. Geophys. Res. Atmos., 119, 5079–5103, doi:10.1002/2013jd020968.

Vachon, R. W., J. M. Welker, J. W. C. White, and B. H. Vaughn, 2010: Moisture source temperatures and precipitation $\delta^{18}O$-temperature relationships across the United States. Water Resources Research, 46 (7), W07523.

Vertenstein, and S. Yeager. 2010. The Parallel Ocean Program (POP) Reference Manual, Ocean Component of the Community Climate System Model (CCSM). Tech. Rep., Los Alamos National Labora- tory Tech. Rep. LAUR-10-01853.

Wadley, M., G. Bigg, E. Rohling, and A. Payne, On modelling present-day and last glacial maximum oceanic !18O distributions, *Global and Planetary Change*, *32*(2-3), 89–109, 2002.

Wang, Y. J., H. Cheng, R. L. Edwards, Z. S. An, J. Y. Wu, C. C. Shen, and J. A. Dorale, 2001: A high-resolution absolute-dated Late Pleistocene monsoon record from Hulu Cave, China. Science (80-.)., 294, 2345–2348, doi:DOI 10.1126/science.1064618.

Werner, M., P. M. Langebroek, T. Carlsen, M. Herold, and G. Lohmann, Stable water isotopes in the ECHAM5 general circulation model: Toward high-resolution isotope modeling on a global scale, *Journal of Geophysical Research-Atmospheres*, *116*(D15), 2011.

Werner, M., B. Haese, X. Xu, X. Zhang, M. Butzin, and G. Lohmann (2016). Glacial–interglacial changes in $H_2{}^{18}O$, HDO and deuterium excess – results from the fully coupled ECHAM5/MPI-OM Earth system model. *Geoscientific Model Development*. **9**, 647-670, doi: 10.5194/gmd-9-647-2016.

Wong, T. E. (2016), The Impact of Stable Water Isotopic Information on Parameter Calibration in a Land Surface Model, Applied Mathematics Graduate Theses & Dissertations. 72. https://scholar.colorado.edu/appm_gradetds/72

Wong, T., Nusbaumer, J., and D. C. Noone (2017). Evaluation of modeled land-atmosphere exchanges with a comprehensive water isotope fractionation scheme in version 4 of the Community Land Model (CLM4). *Journal of Advances in Modeling Earth Systems*. **9**, Issue 2, 978-1001, doi: 10.1002/2016MS000842.

Zachos, J. C., M. Pagani, L. Sloan, E. Thomas, and K. Billups, 2001: Trends, Global Rhythms, Aberrations in Global Climate 65Ma to Present. Science (80-.)., 292, 686–693, doi:10.1126/science.1059412.

Zhang, J., Z. Liu, E. C. Brady, A. Jahn, K. Lindsay, D. W. Oppo, P. U. Clark, S. A. Marcott, 2017: Asynchronous warming and $\delta^{18}O$ evolution of deep Atlantic water masses during the last deglaciation, PNAS, doi:10.1073/pnas.1704512114

Zhu, J., and Coauthors, 2017a: Reduced ENSO variability at the LGM revealed by an isotope-enabled Earth system model. Geophys. Res. Lett., 44, 6984–6992, doi:10.1002/2017GL073406.

Zhu, J., and Coauthors, 2017b: Investigating the direct meltwater effect in terrestrial oxygen-isotope paleoclimate records using an isotope-enabled Earth system model. Geophys. Res. Lett., 44, 12501–12530, doi:10.1002/2017GL076253.

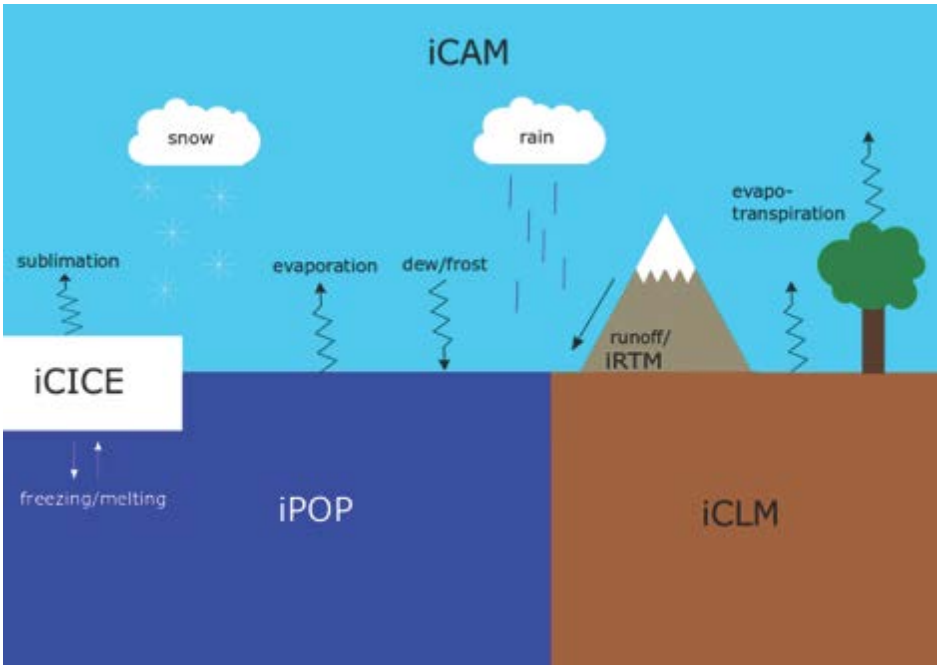

Figure 1. A schematic of iCESM1 showing the five major model components (iCAM, iCLM, iRTM, iPOP, and iCICE) and all of the major inter-component fluxes that impact water isotopes. It should be noted that although some of these fluxes are only shown once, they occur for multiple components (e.g. dew/frost can occur between iCAM and iCLM, iPOP, and iCICE).

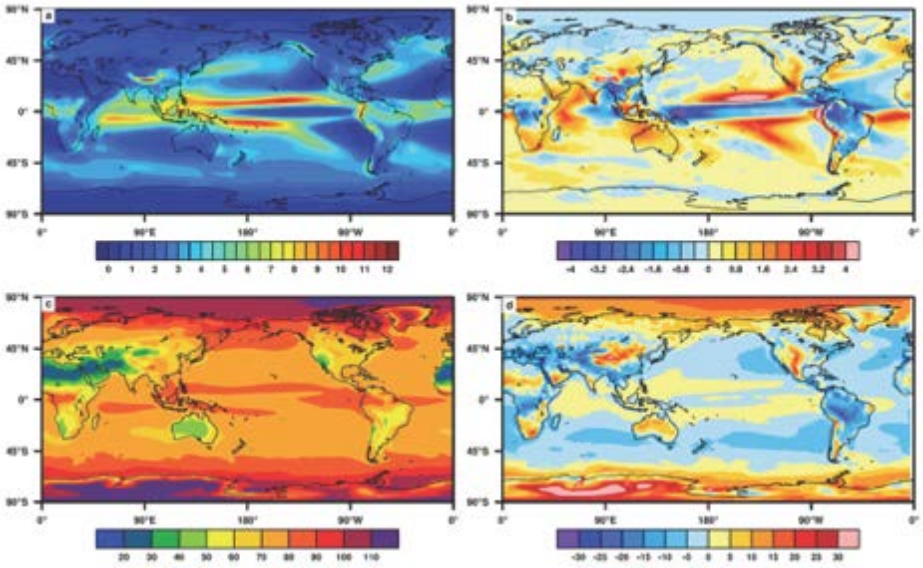

Figure 2. Annual average precipitation in mm/day (a) and surface relative humidity in percent (c) as simulated by iCESM1. Also shown are the differences between iCESM and ERA-Interim for precipitation (b) and surface relative humidity (d). The iCESM values were averaged over model years 1950-2005.

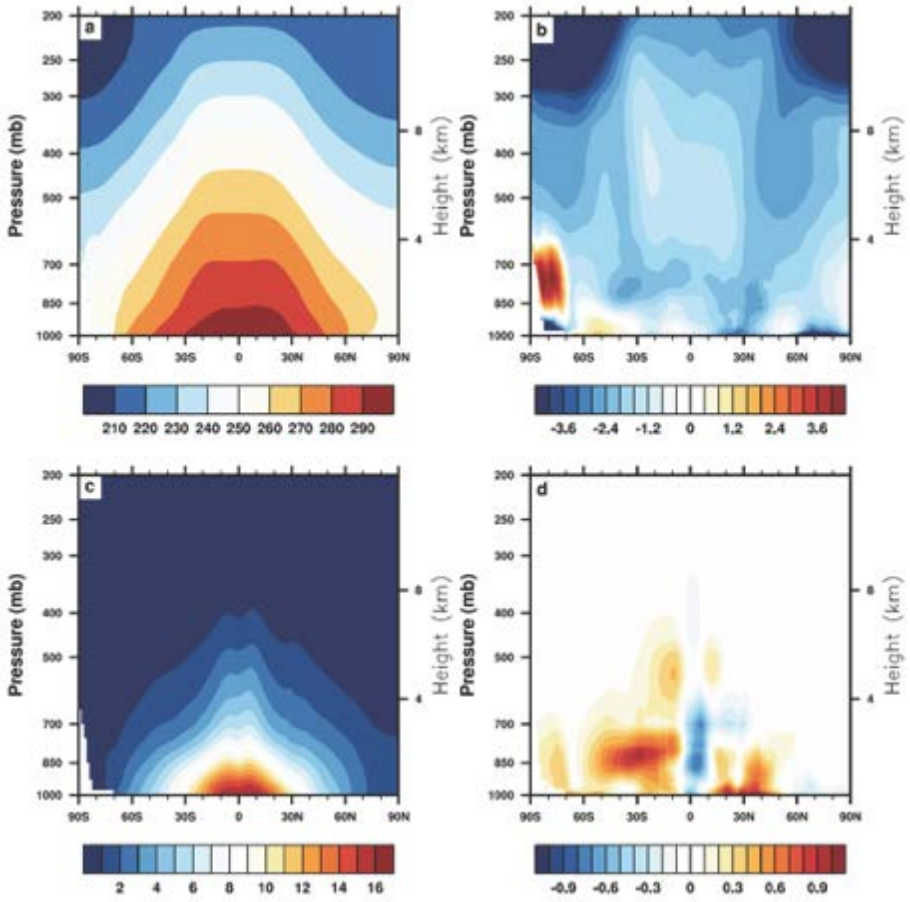

Figure 3. Zonal and annual average air temperature in Kelvin (a) and specific humidity in g/kg (c) as simulated by iCESM1.2. Also shown are the differences between iCESM and ERA-Interim for air temperature (b) and specific humidity (d). The iCESM values were averaged over model years 1950-2005.

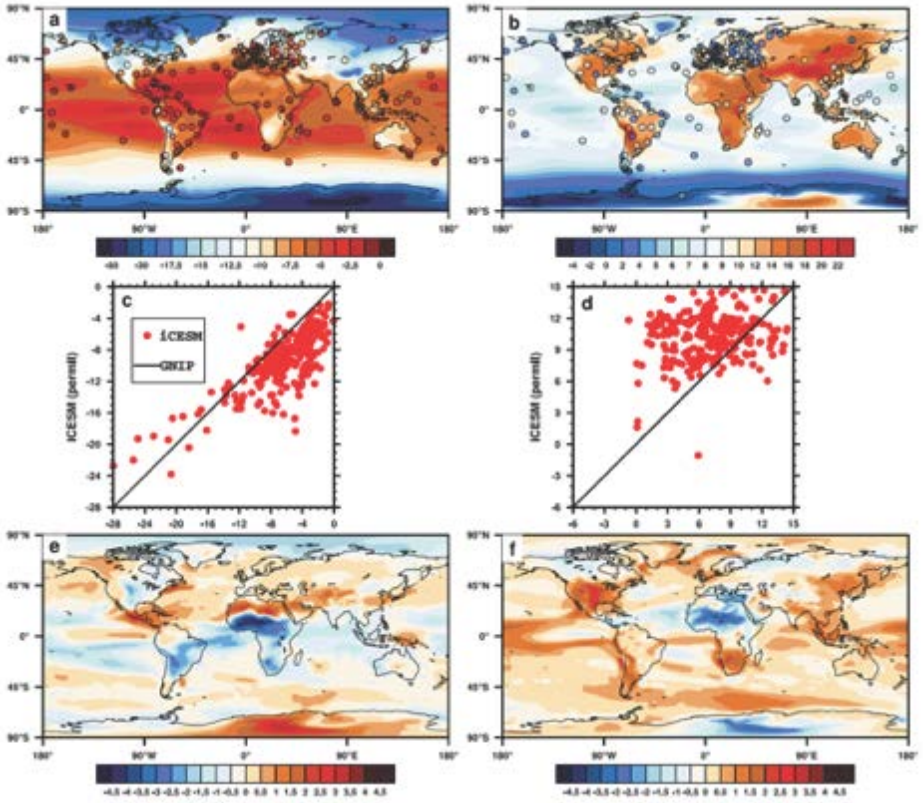

Figure 4. Annual average precipitation $\delta^{18}O$ (a) and d-excess (b) from iCESM1.2 (contours) and GNIP (circles). Also shown are the average $\delta^{18}O$ (c) and d-excess (d) values from the model grid cells closest to each GNIP station, compared against those GNIP values. The black line shows the values for a "perfect" match with GNIP. The differences between iCESM1.2 and iCAM5/iCLM4 with prescribed SSTs are also shown for precipitation $\delta^{18}O$ (e) and d-excess (f). The iCESM1.2 values were averaged over model years 1950–2005. The iCAM5 and GNIP values were the same used in Nusbaumer et al. (2017).

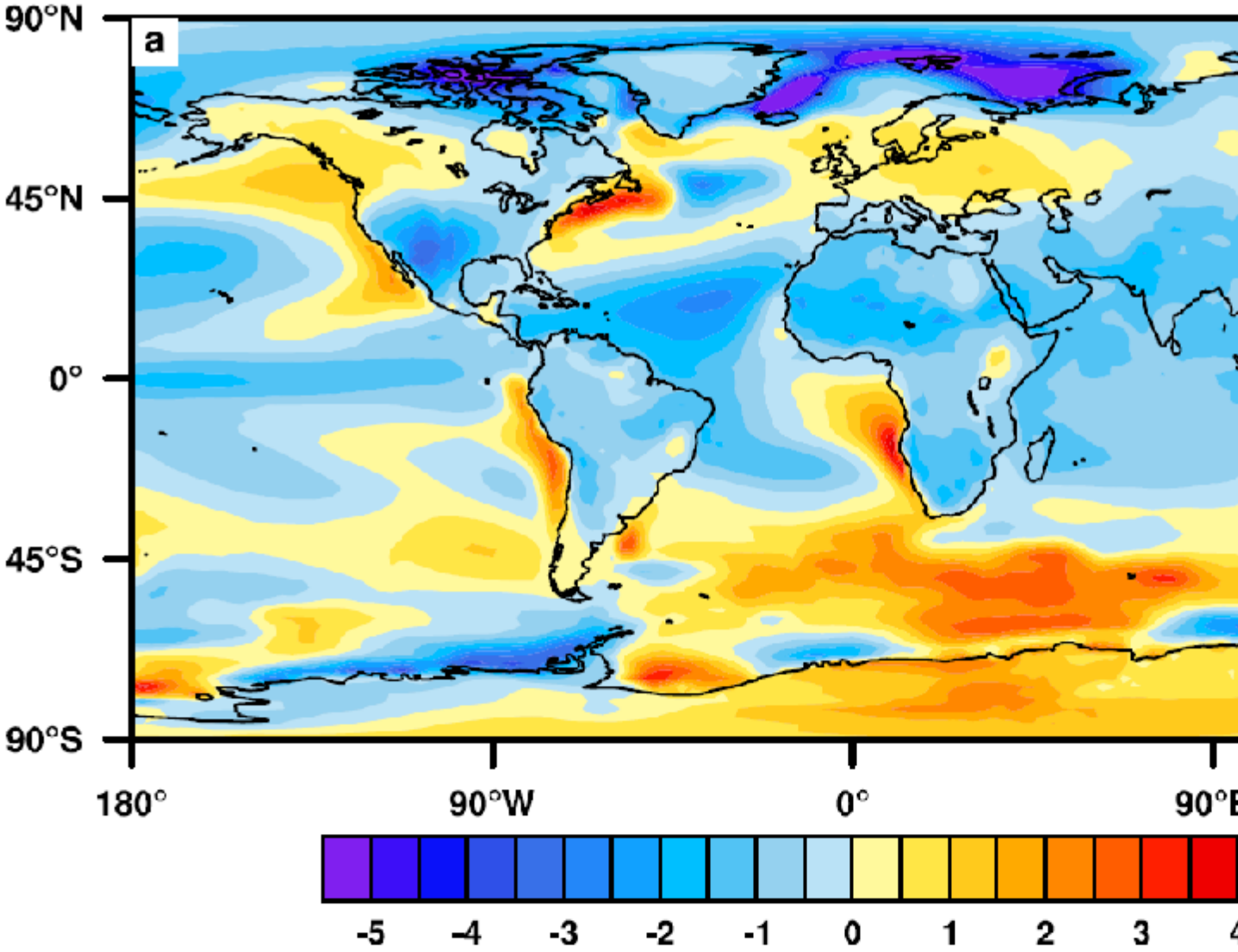

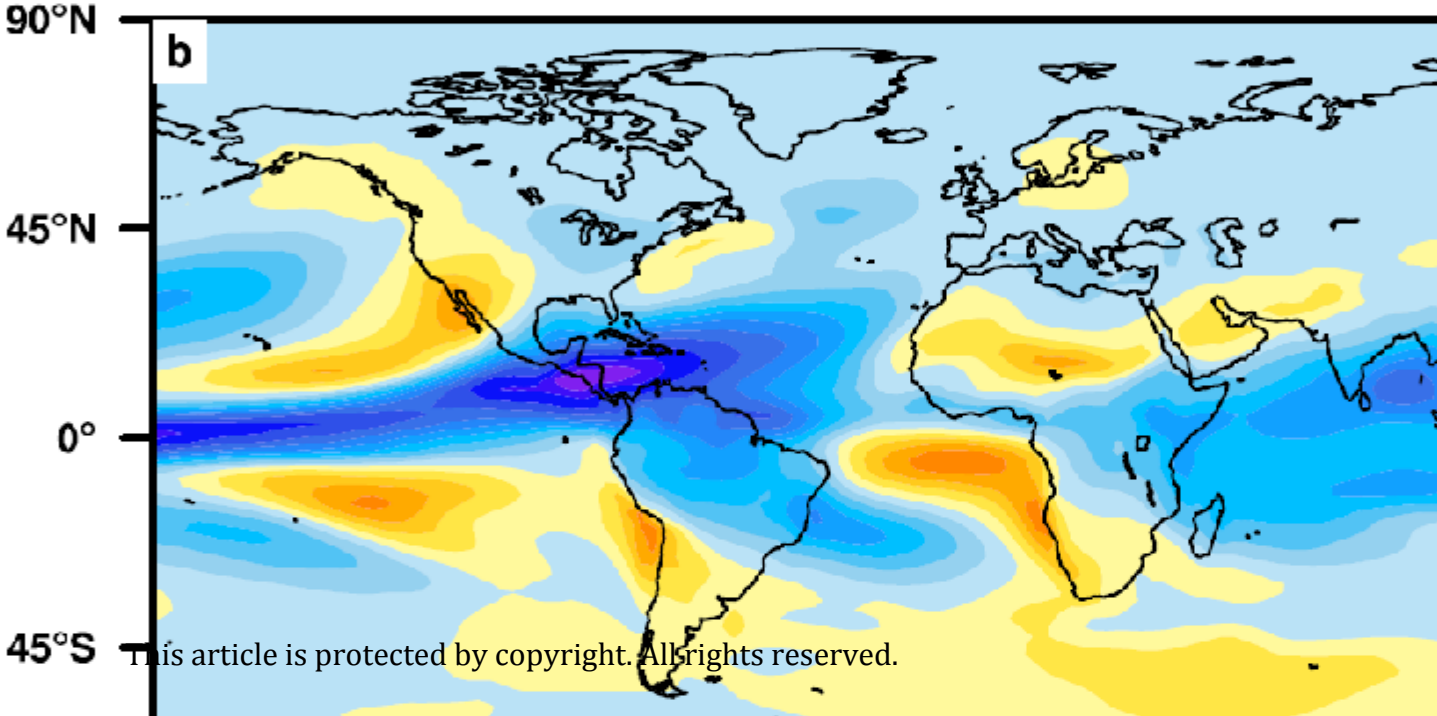

Figure 5. Climatological differences in (a) surface temperature, defined here as the temperature at the lowest atmospheric model layer, (b) precipitable water, and (c) evaporation minus precipitation, between iCESM1 and iCAM5/iCLM4 with prescribed SSTs and sea ice.

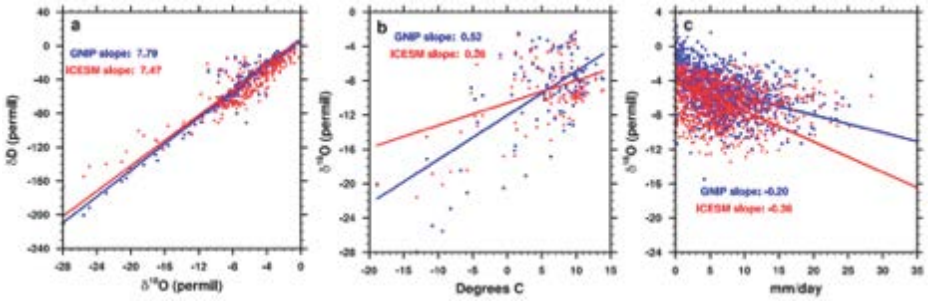

Figure 6. Scatter plots of time-averaged precipitation-weighted $\delta^{18}O$ and δD (a), surface air temperature and $\delta^{18}O$ of precipitation in the extra tropics (b), and precipitation rate and $\delta^{18}O$ of precipitation in the tropics (c) for GNIP (blue) and iCESM (red) at the grid-cell nearest to the GNIP station. The solid lines represent the linear regression between the respective quantities, with the slopes of those regression lines shown in the legends for both GNIP and iCESM. The temperature plot (b) only uses stations poleward of 45° N/S, whereas the precipitation plot (c) only uses stations between 15° N/S and 90° E to 255° E. The precipitation plot also uses monthly values, while all other plots use the long-term averages for each station.

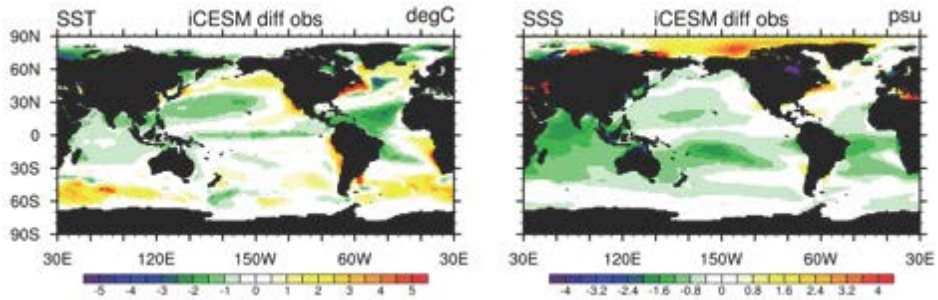

Figure 7. Model annual mean **(a)** sea surface temperature (SST) and **(b)** sea surface salinity (SSS), minus the WOA13v2 observational climatology (Boyer et al. 2013). The model results are averaged over years 1955–2005. Biases are in degrees Celsius and PSU, respectively.

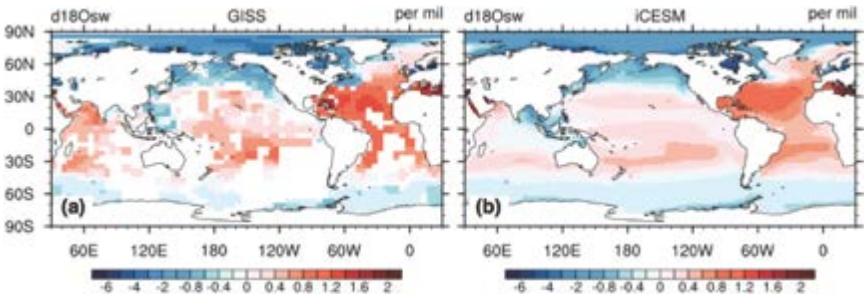

Figure 8. Model-data comparison of annual mean $\delta^{18}O$ composition of surface seawater (units: ‰). **(a)** the GISS data set and **(b)** iCESM simulation (1955–2005).

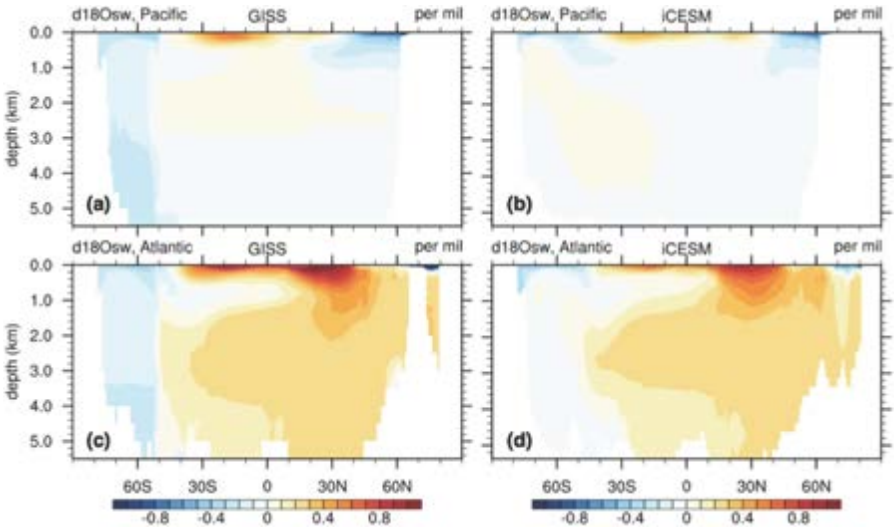

Figure 9. Model-data comparison of zonal mean seawater $\delta^{18}O$ (units: ‰). Pacific zonal mean in the GISS data set **(a)** and the iCESM simulation **(b)** averaged between year 1955 and 2005. **(c)** and **(d)** As **(a)** and **(b)** but for the Atlantic zonal mean.

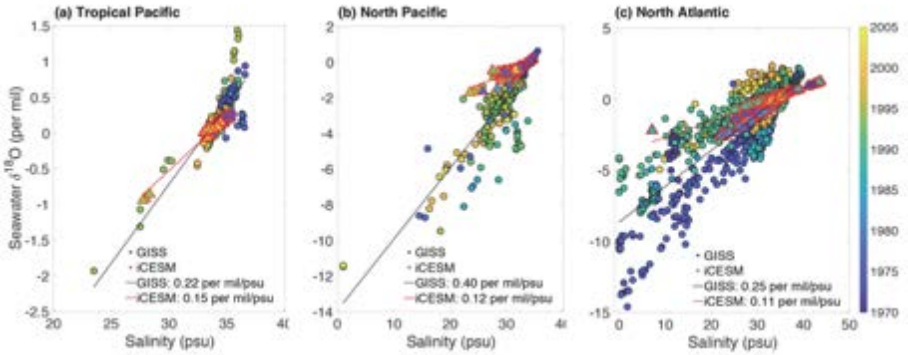

Figure 10. Relationship between salinity and seawater $\delta^{18}O$, in both iCESM and the GISS database. Color shading indicate the model year of the simulation. Circles indicate GISS data and triangles iCESM output. Note that iCESM output has been subsampled to match the lats/lons/times corresponding to GISS data points; best-fit regressions for GISS and iCESM are plotted as black and red lines, respectively. **(a)** Tropical Pacific (25S-25N, 90E-90W); **(b)** North Pacific (30-70N, 90E-90W); **(c)** North Atlantic (0-70N, 100W-60E).

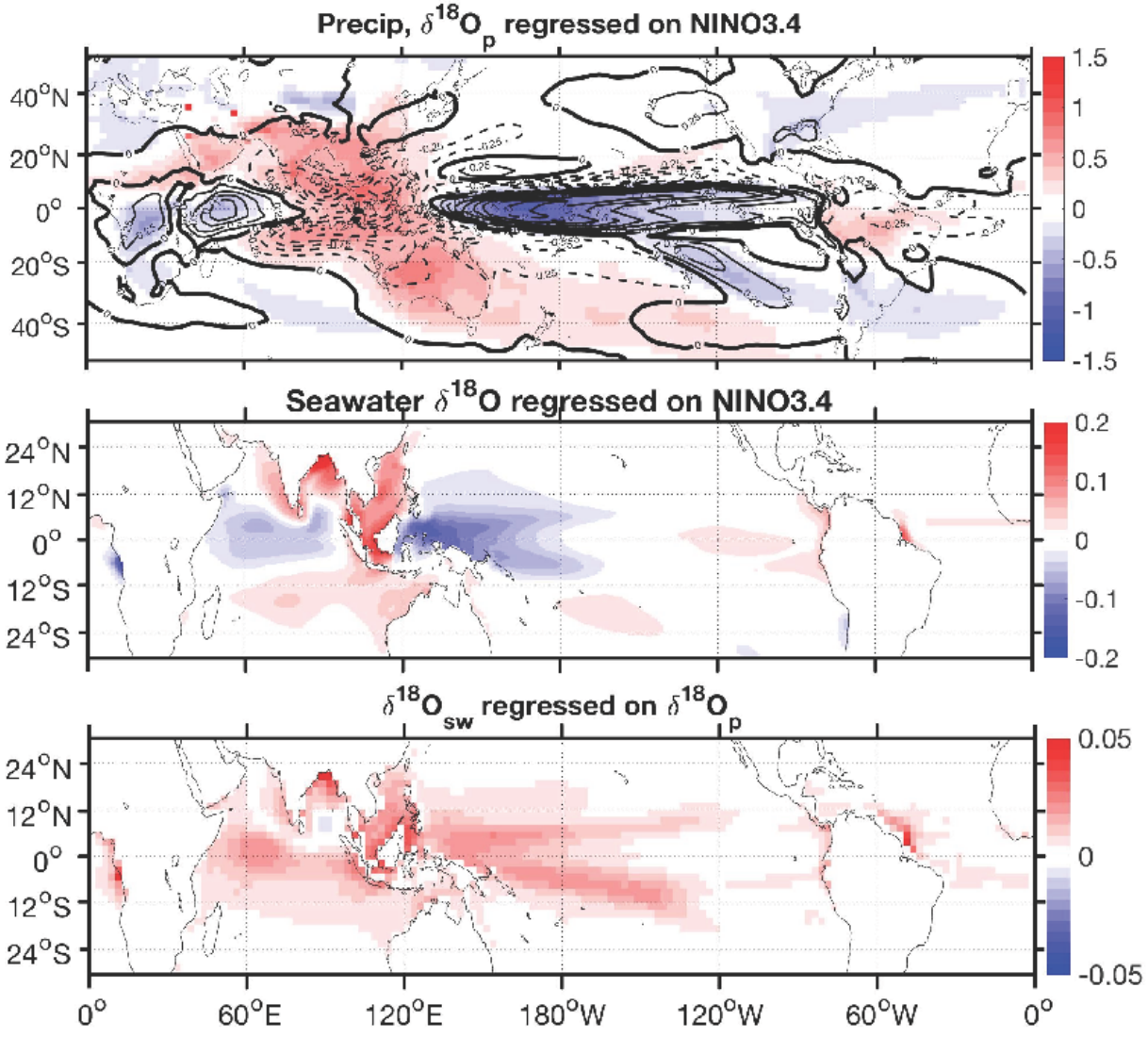

Figure 11: a) Anomalies in precipitation (contours), $\delta^{18}O$ of precipitation (colors) regressed on NINO3.4 SSTA in iCESM. Time period is the entire length of an iLME full-forcing experiment (850-2005), and anomalies are all computed relative to a 20-year moving window. b) Same as a), for seawater $\delta^{18}O$ anomalies. c) Regression of gridpoint seawater $\delta^{18}O$ on precipitation $\delta^{18}O$ anomalies. Time period and anomaly computation is the same as in a).

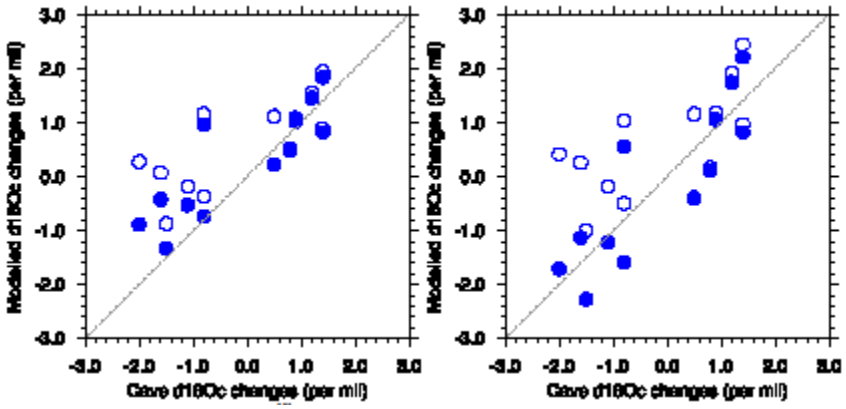

Figure 12: A model-data comparison of response in speleothem $\delta^{18}O$ during Heinrich Events (units: ‰). The response in the model is the difference between a water hosing experiment and a preindustrial control simulation. Either 0.25 Sv (left) or 0.5 Sv (right) freshwater with a $\delta^{18}O$ signature of [illegible] results if only the indirect climate effects are considered (no influence from meltwater $\delta^{18}O$); filled circles include both effects. Modelled $\delta^{18}O_c$ is calculated from model $\delta^{18}O_p$ and temperature using Kim and O'Neil (1997). Reproduced from Zhu et al. (2017b), Fig S3. Please refer to Zhu et al. (2017b) for details of the simulations and model-data comparison.

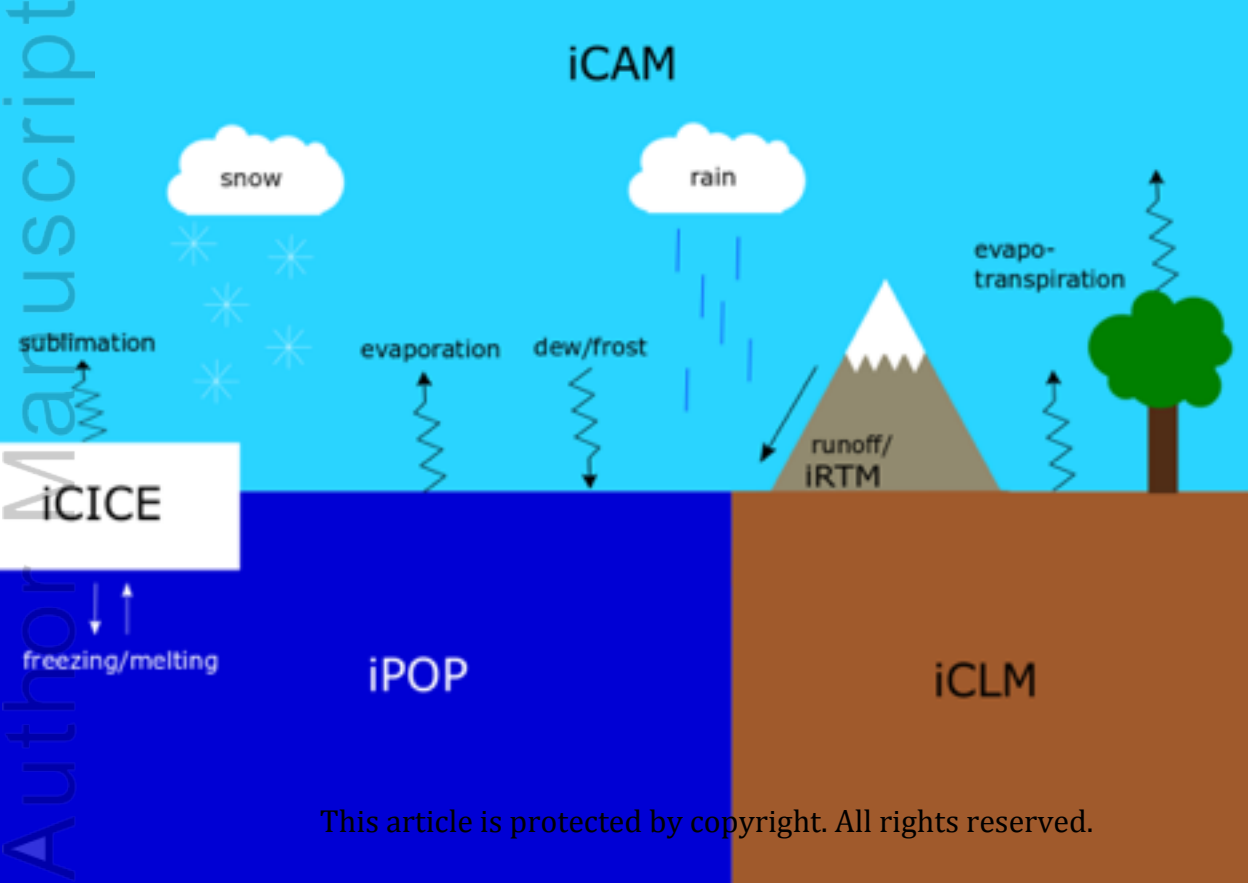

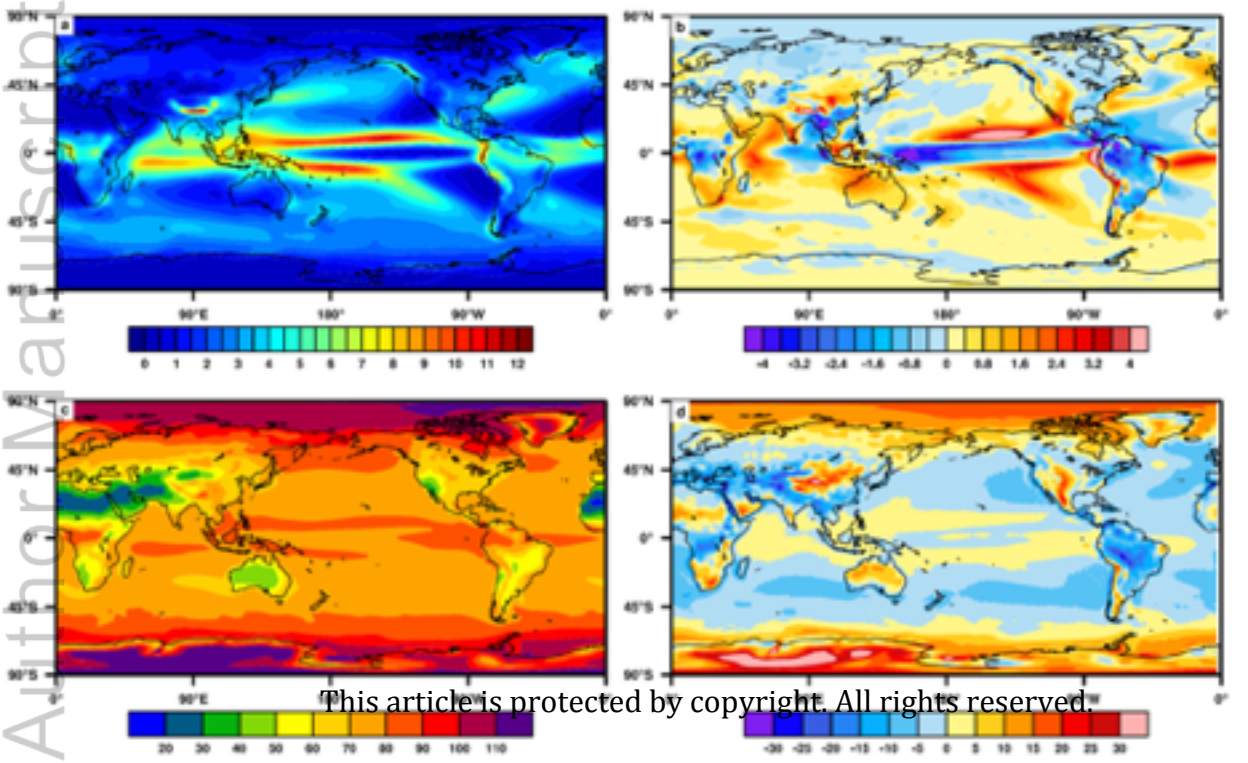

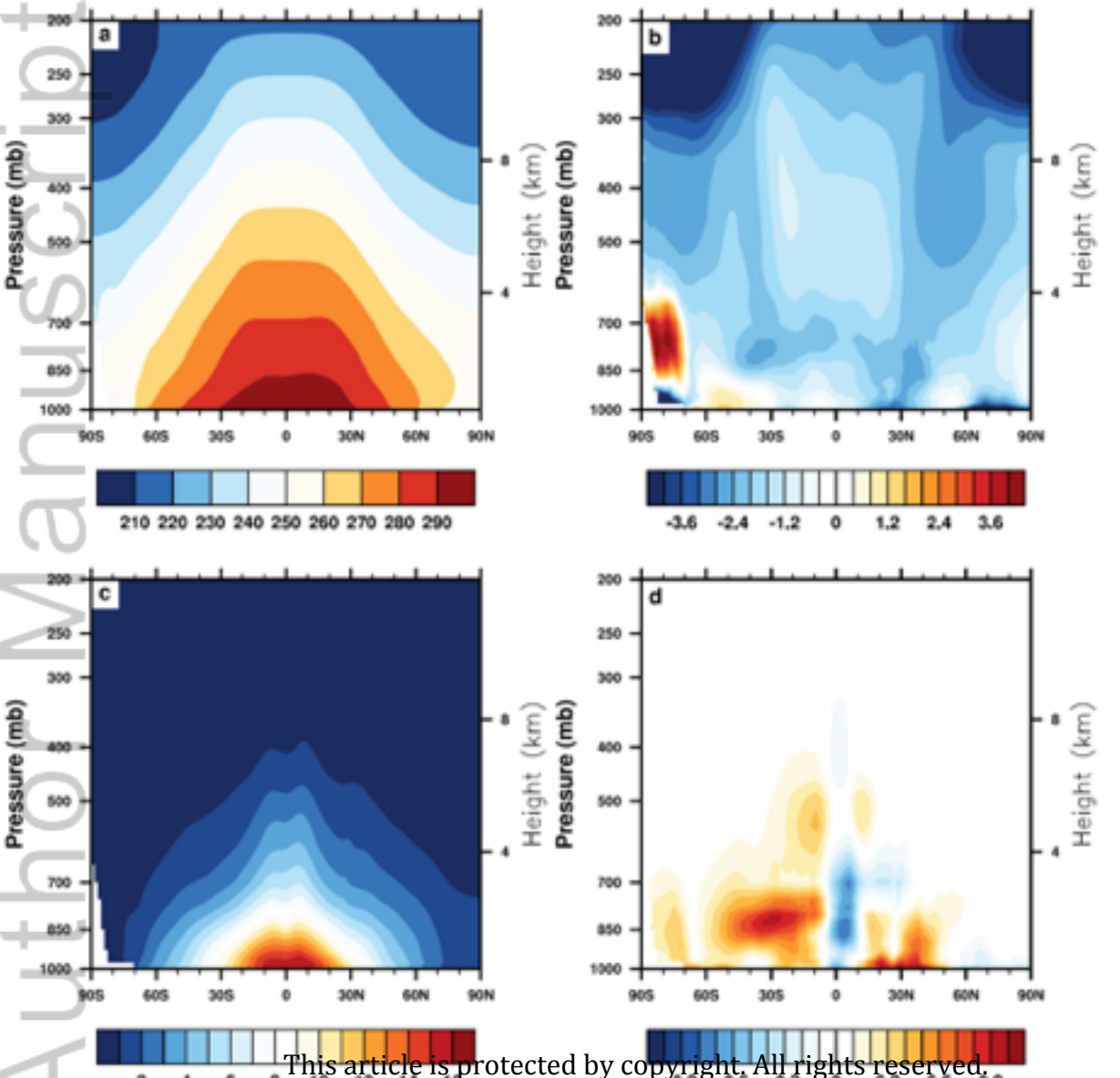

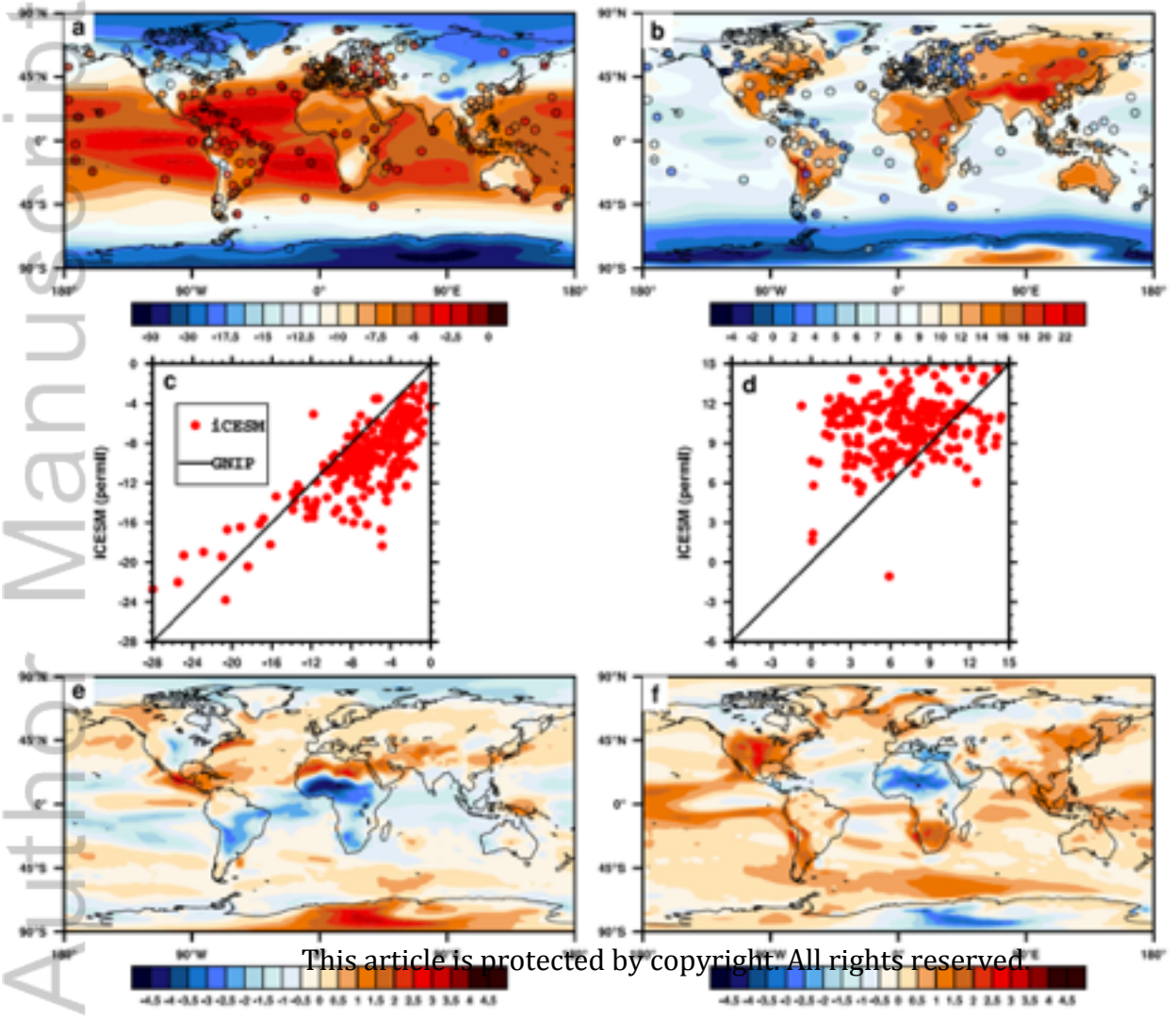

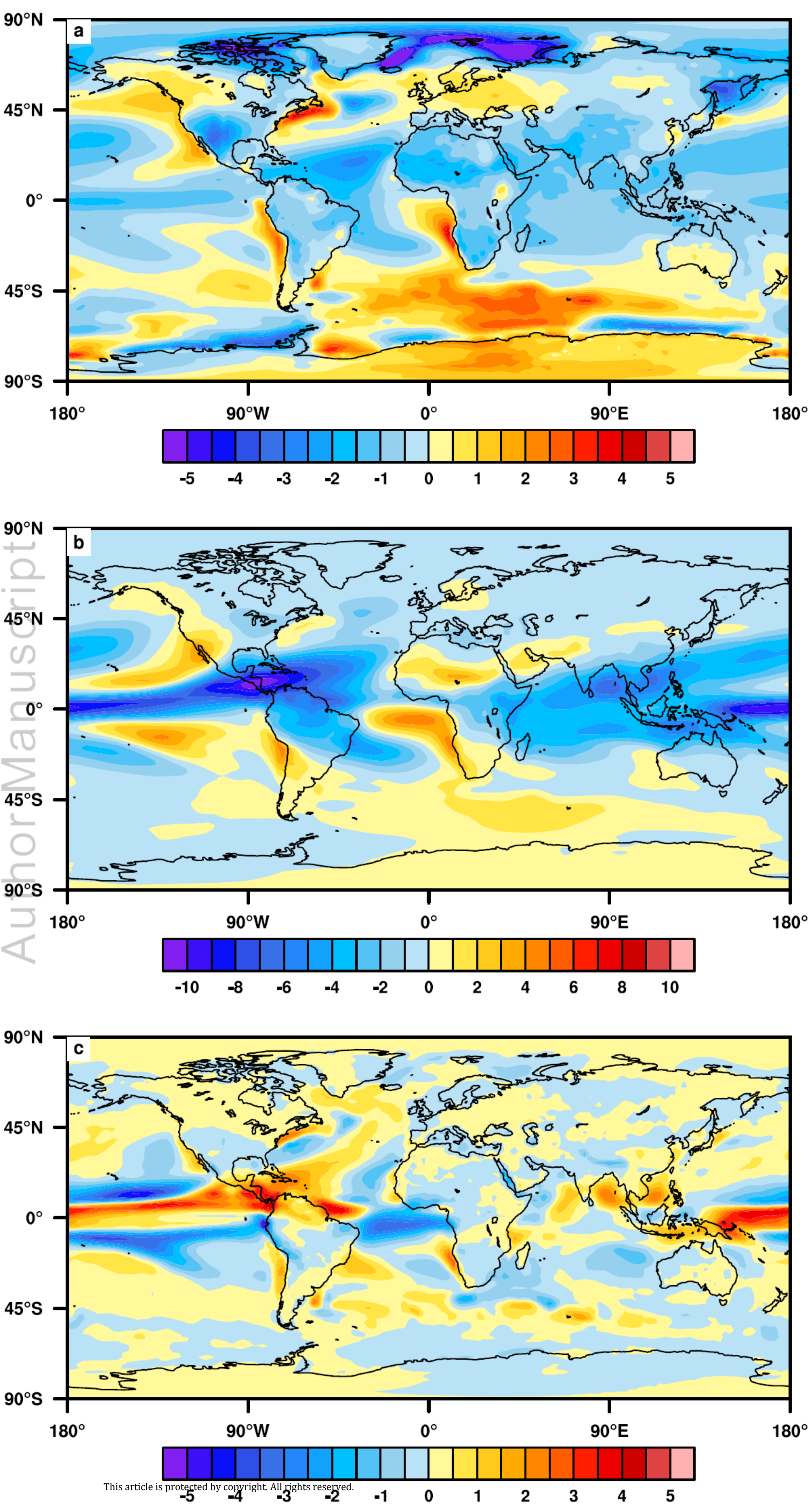

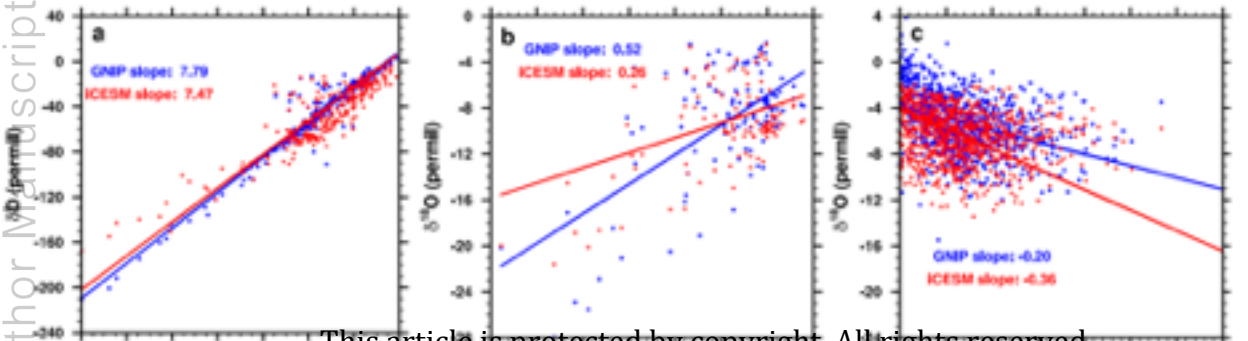

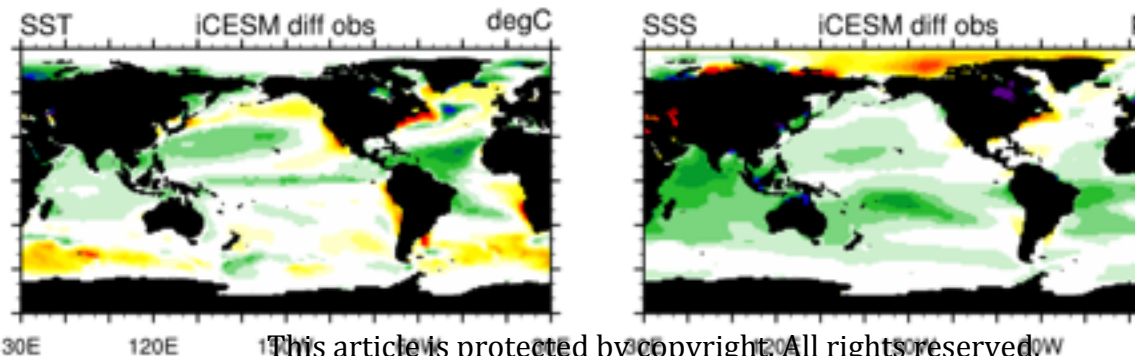

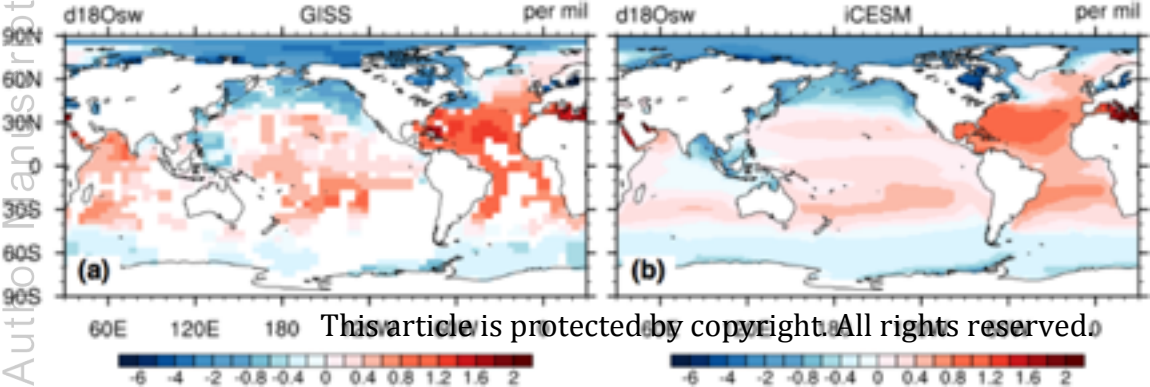

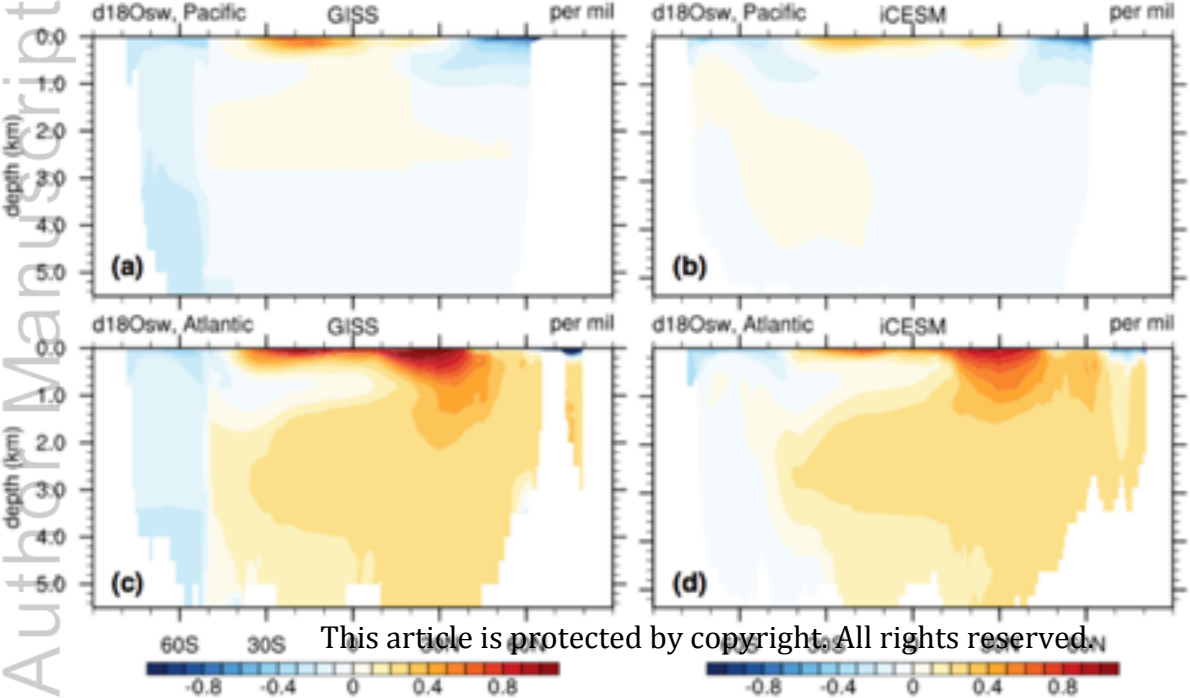

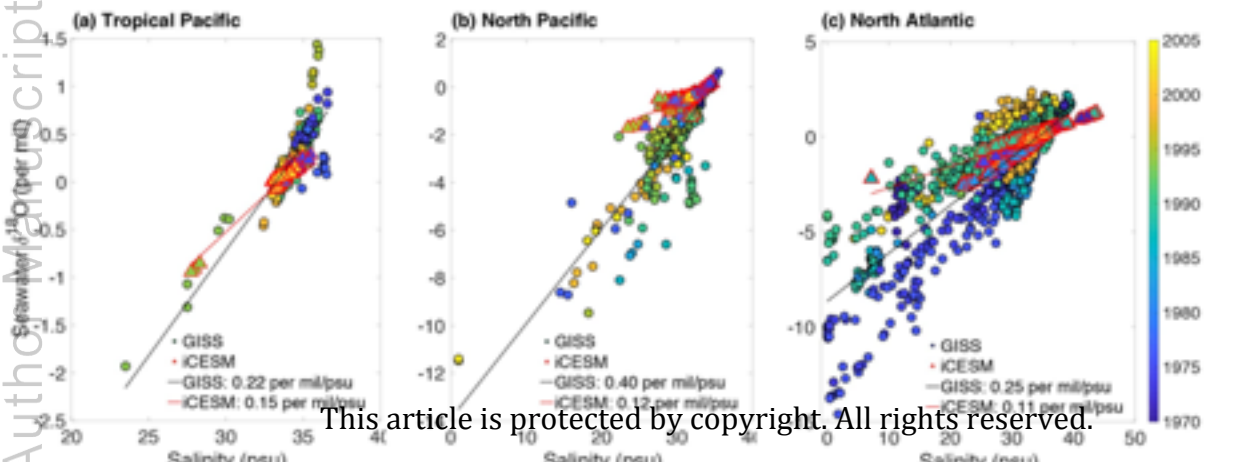

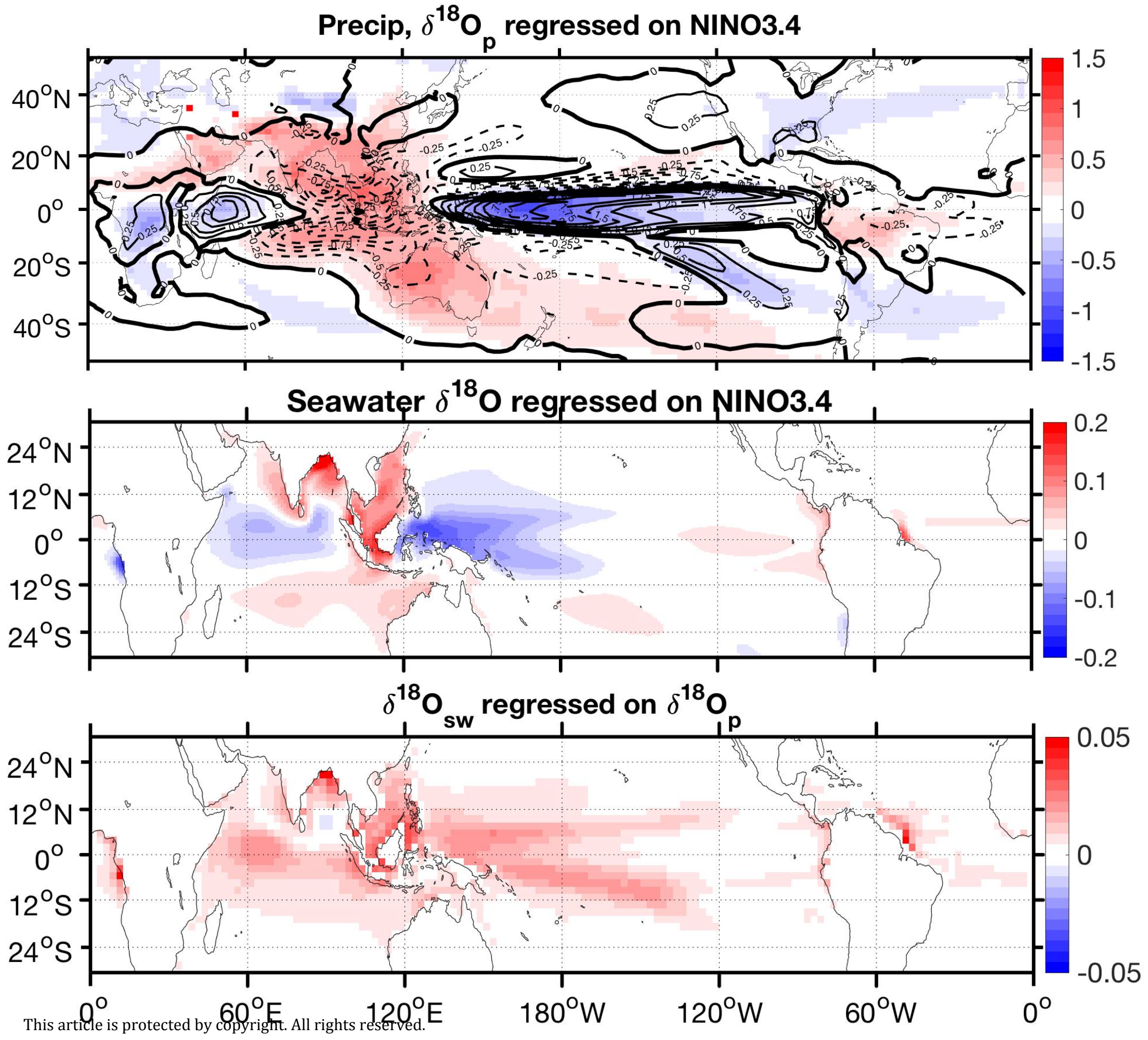

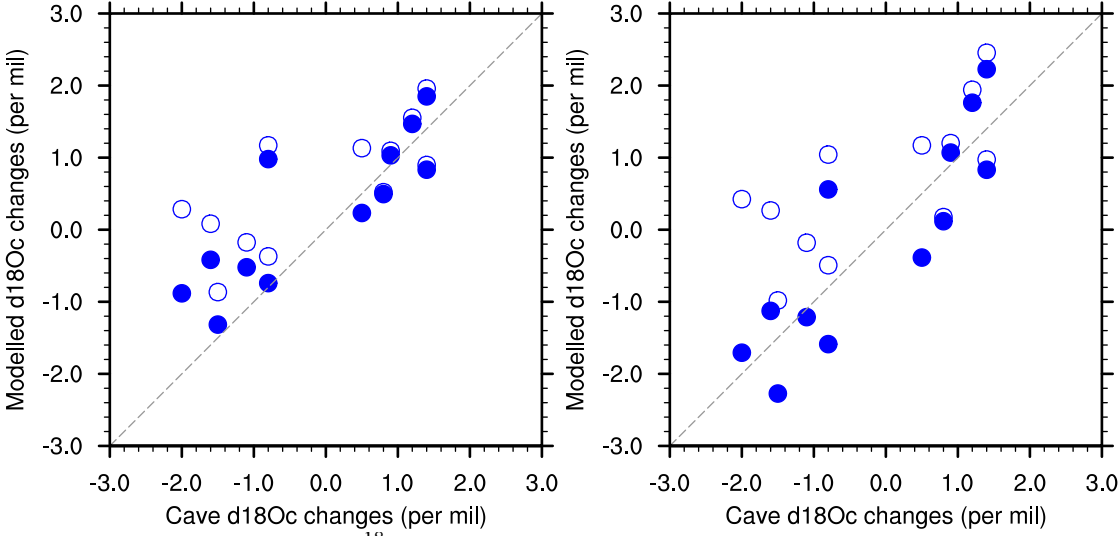
Modelled d18Oc changes (per mil)
Cave d18Oc changes (per mil)
3.0
2.0
1.0
0.0
-1.0
-2.0
-3.0
-3.0
-2.0
-1.0
0.0
1.0
2.0
3.0
Modelled d18Oc changes (per mil)
Cave d18Oc changes (per mil)